# Soil Moisture Retrieval During Crop Growth Cycle Using Satellite SAR Time Series

Arnab Muhuri, Kalifa Goïta, Ramata Magagi, and Hongquan Wang

***Abstract*—Satellite SAR-based soil moisture retrieval over agricultural fields, under crop overlain conditions, is a challenging exercise. This is so because the overlying crop volume interacts with both the incoming and the backscattered radar signal. Therefore, the soil moisture linked solely to the top layer (0–5 cm) of the soil cannot be reliably retrieved under such conditions without avoiding the obscuring effect of growing crop volume. In this investigation, we demonstrated a proof-of-concept for a time-series approach to retrieve soil moisture during crop growth cycle. Contrary to the use of the single-scene approach, the novelty of the proposed approach lies in exploiting the satellite SAR time series acquired during a cropping cycle. The proposed time-series approach is effective for capturing the nuances in the crop phenological stages while calibrating the Dubois–water cloud model (WCM) soil moisture retrieval model. By employing this approach, we achieved the 0.04 $m^3$ $m^{-3}$ soil moisture retrieval root-mean-square error benchmark at a high spatial resolution and addressed the issue of solving for the Dubois–WCM model constants under data-constrained conditions. Furthermore, we observed that the combination of temporally non-overlapping vegetation descriptors (optical and SAR) resulted in degradation in the performance of the retrievals and under such circumstances single polarimetric descriptor performed better.**

***Index Terms*—Dubois model, polarimetric SAR, RADARSAT-2 (RS2), soil moisture retrieval, water cloud model (WCM).**

## I. Introduction

CLIMATE change is expected to have a severe impact on the global agricultural ecosystem [1]. Among the various environmental and societal aspects that climate change is expected to affect, it will impact soil moisture, which is one of the vulnerable factors from the socioeconomic perspective. Soil moisture is an important water resource since it supports a significant percentage of the global food production and determines the crop productivity.

Passive microwave sensors, such as soil moisture active passive (SMAP) and soil moisture ocean salinity, offer the possibility to observe soil moisture on a global scale at a reasonably high temporal resolution. However, the spatial scale (radiometer: 40 km) of the insights provided by the data from these sensors is limited to farm-level (1 km or a few hundred meters) agricultural management practices [2], [3]. Recent investigations indicate a growing interest toward SAR-based high-resolution soil moisture products for either downscaling the coarse-resolution passive microwave products (active–passive synergy) or solely employing the data from SAR missions, such as Sentinel-1 and RADARSAT-2 (RS2) [4], [5].

A seminal investigation synergistically merged passive microwave data from SMAP and AMSR2 radiometers with the active Sentinel-1 SAR data using a disaggregation technique based on smoothing filter-based intensity modulation that resulted in compensation for the failure of SMAPs active radar sensor and soil moisture map at an enhanced ($\approx$ 10 km) resolution [6]. A recent investigation adopted a well-established change detection algorithm to propose a globally deployable soil moisture observation at 1 km resolution using the Sentinel-1 satellites. The investigation employed a novel dynamic Gaussian upscaling method for spatially upscaling the SAR images and mitigating the SAR signal complexity [7]. The multitemporal least square moisture estimator software was implemented with an automated processing chain for providing high-resolution ($\approx$ 500 m) operational service over Italy. The service exploited the Sentinel-1 time-series and ancillary data (e.g., plant water content map) for mapping soil moisture at the national scale [8]. Another investigation conceived a similar operational service by implementing the soil moisture multitemporal algorithm based on the Bayesian maximum *a posteriori* probability statistical criterion to exploit the benefits of the short revisit time of Sentinel-1 time series (such as surface roughness remains relatively unchanged as compared with soil moisture) [9], [10]. Investigations also highlighted the merits of satellite time series in terms of addressing the ill-posed problem of soil moisture retrieval, compensating for the vegetation effects, and the feasibility of using retrieval techniques based on change detection and Bayesian approaches [11], [12]. An investigation utilized multitemporal *L*-band SAR data (acquired at HH polarization) for

Manuscript received 19 March 2023; revised 27 April 2023 and 17 May 2023; accepted 21 May 2023. Date of publication 26 May 2023; date of current version 16 October 2023. This work was supported in part by the Natural Science and Engineering Research Council of Canada (NSERC) Discovery under Grant RGPIN-2017-05533 and Grant RGPIN-2018-06101, in part by Collaborative Research and Training Experience (CREATE) under Grant 543360-2020, and in part by the Canadian Space Agency Class Grant and Contribution Program under Grant 21SUESAMMI as part of the Canadian plan to spatial missions of soil moisture. *(Corresponding author: Arnab Muhuri.)*

Arnab Muhuri was with the Centre d'Applications et de Recherches en Télédétection, Département de Géomatique Appliquée, Université de Sherbrooke, Sherbrooke, QC J1K 2R1, Canada. He is now with the Earth Observation and Modelling, Geographisches Institut, Christian-Albrechts-Universität zu Kiel, 24118 Kiel, Germany (e-mail: muhuri@geographie.uni-kiel.de).

Kalifa Goïta and Ramata Magagi are with the Centre d'Applications et de Recherches en Télédétection, Département de Géomatique Appliquée, Université de Sherbrooke, Sherbrooke, QC J1K 2R1, Canada (e-mail: kalifa.goita@usherbrooke.ca; ramata.magagi@usherbrooke.ca).

Hongquan Wang was with the Centre d'Applications et de Recherches en Télédétection, Département de Géomatique Appliquée, Université de Sherbrooke, Sherbrooke, QC J1K 2R1, Canada. He is now with the Lethbridge Research and Development Centre, Agriculture and Agri-Food Canada (AAFC), 5403 1 Ave S, Lethbridge, AB T1J 4B1, Canada (e-mail: Hongquan.Wang@USherbrooke.ca).

Digital Object Identifier 10.1109/JSTARS.2023.3280181

retrieving superficial soil moisture by inverting the IEM surface scattering model using a constrained optimization technique. The approach required *a priori* information on soil parameters, such as soil moisture predictions, at a coarser resolution for high-resolution SAR retrievals [11]. Furthermore, the adopted approach disregarded the presence of vegetation by arguing that at the *L*-band and HH polarization, there is a reduced sensitivity of backscatter to the fresh crop biomass and the important contribution comes from the soil and its moisture variations. A recent investigation considered the time-varying nature of the vegetation and approximated its effect on the *C*-band Sentinel-1 radar backscatter. However, it still indicated a dependency on a temporal soil moisture constraint based on coarse SMAP soil moisture product to partly remove the uncertainties caused by time-varying vegetation and/or roughness [13].

Over the past decade, several SAR-based soil moisture retrieval investigations have demonstrated performances approaching/achieving the 0.04 $m^3$ $m^{-3}$ root-mean-square error (RMSE) benchmark [14], [15], [16]. The retrieval methodologies varied from model based (Oh, Dubois, IEM, etc.) to machine learning based (ANN, SVR, RF etc.) approaches [17], [18] and the choice of SAR sensors for these investigations ranged from full to compact polarimetric [19], [20]. Investigations have reported the performances of machine learning based retrievals to be commendable when implemented with simulation derived from forward electromagnetic models for generating training datasets since they provide a physical justification and avoid the issue of "black box" algorithm [21]. Such physical justifications are provided well by the model-based approaches, which are formulated based on empirical/semi-empirical/physical pieces of evidence (such as Maxwell's equations) and not merely dedicated for recognizing any arbitrary pattern. Such models provide a physics-based description of the electromagnetic interactions of the microwave imaging signal with terrestrial targets, such as bare or vegetated soil [22]. Upon comparing the performance of neural network approaches and statistical methods based on Bayesian procedures, the former approach was observed to have a better performance with more inputs (multiple polarizations and incidence angles) in the training phase [23]. The contribution of [24] is commendable in this direction since the investigation achieved an impressive soil moisture retrieval RMSE of 0.023 $m^3$ $m^{-3}$ by implementing a retrieval algorithm based on an artificial neural network (a feedforward multilayer perceptron) approach. The investigation utilized a time series of ENVISAT/ASAR images, where the effect of vegetation was accounted for by using the water cloud model (WCM) with normalized difference vegetation index (NDVI) information. By considering the impracticality of obtaining the surface roughness parameters (for the scattering models) for large-scale applications, machine learning approaches are frequently acknowledged as reasonable options [25]. Furthermore, a comparison between model-based and machine learning based retrievals revealed that the performance of the latter was encouraging and comparable to those obtained by the scattering models.

Despite the availability of a choice of soil moisture retrieval models, a number of factors constrain their operational use with active SAR data [26], [27]. Growing vegetation and soil roughness influence the backscattered radar signal leading to challenging retrieval scenarios [28]. In addition to this, the response of subsurface roughness due to radar signal penetration at certain wavelengths further complicates the issue, which is variable (depending on crop water content and incidence angle) and not easily quantifiable. Moreover, the mathematical formulation of surface roughness in such models does not satisfactorily represent the natural surface [29], [30]. Such limitations for *a priori* knowledge of the surface roughness information have been addressed by investigations employing a simplified expression of the Dubois model. The simplification is based on the multipolarization inversion scheme that explicitly defines the real dielectric constant as a function of co-polarized backscattering coefficients and the imaging sensor parameters [14]. An investigation successfully utilized this simplified expression, parameterized with the WCM, and retrieved soil moisture with the quad-pol RS2 and dual-pol TerraSAR-X data over prairie landscapes without any *a priori* knowledge of surface roughness [31].

In this investigation, we demonstrated a proof-of-concept for a time-series approach to retrieve soil moisture during crop growth cycle. The uniqueness of the proposed technique lies in the manner the multitemporal satellite SAR datasets were employed to calibrate the retrieval model and assess the performance. Unlike the conventional approach for estimating the model constants by spatially sampling a single satellite SAR scene [31], we exploited the time series of full-polarimetric RS2 scenes covering crop growth cycles in order to capture the nuances in the phenological variations. The time series utilized in this investigation covered cropping cycles from 2012 and 2016 over the agricultural fields in Carman, Manitoba, Canada. The approach employed the simplified empirical Dubois model (that addressed the surface roughness constraint) in conjunction with the WCM (that compensated for the vegetation scattering) [32], [33]. The parameterized model was calibrated by dedicating a subset of the time series. An unbiased assessment of the performance of soil moisture retrievals was observed with the remaining scenes as well as scenes belonging to a different cropping period. The latter was achieved by transferring the calibrated model constants for retrievals from fields of the same crop type. This investigation highlighted the impact of, simultaneously, combining polarimetric and optical vegetation descriptors (with some temporal latency).

## II. Test Site and Data

### A. Test Site

Carman is an important agricultural hub in Manitoba, Canada. The region is located in the middle of a rich agricultural belt approximately 90 km west of Winnipeg and 60 km north of the U.S. border at the eastern edge of the Canadian prairies [34]. The topography over the area is generally flat [35]. The presence of farm-based research facilities and a network of soil moisture stations [real-time in situ soil monitoring for agriculture (RISMA)], established by the Agriculture and Agri-Food Canada (AAFC) and Environment and Climate Change Canada, make this site a feasible choice for soil moisture investigations [20], [36], [37].

TABLE I
RS2 TIME-SERIES: IN *2012* AND *2016* OVER CARMAN, MANITOBA, CANADA

| Acquisition Dates | Beam Modes | $\theta_i(\circ)$ | Function |
|---|---|---|---|
| **June 5th (2012)** | FQ3W | 20–23.6 | TV |
| June 12th | FQ8W | 26.1–29.4 | TV |
| June 12th | FQ10W | 28.4–31.6 | TV |
| June 19th | FQ6W | 23.7–27.2 | TV |
| June 26th | FQ2W | 19–22.7 | TV |
| June 29th | FQ3W | 20–23.6 | TV |
| July 6th | FQ8W | 26.1–29.4 | TV |
| July 6th | FQ10W | 28.4–31.6 | TV |
| July 13th | FQ6W | 23.7–27.2 | TV |
| **May 16th (2016)** | **FQ15W** | 33.78–36.37 | **V** |
| May 30th | FQ7W | 24.9–28.3 | BV–TV |
| June 6th | FQ2W | 19–22.7 | BV–TV |
| **June 9th** | **FQ15W** | 33.78–36.37 | **V** |
| June 23rd | FQ7W | 24.9–28.3 | BV–TV |
| June 30th | FQ2W | 19–22.7 | BV–TV |
| July 3rd | FQ15W | 33.78–36.37 | BV–TV |
| July 10th | FQ11W | 29.59–32.70 | BV–TV |
| July 17th | FQ7W | 24.9–28.3 | BV–TV |
| July 24th | FQ2W | 19–22.7 | BV–TV |
| **July 27th** | **FQ15W** | 33.78–36.37 | **V** |
| August 3rd | FQ11W | 29.59–32.70 | BV–TV |
| August 10th | FQ7W | 24.9–28.3 | BV–TV |
| August 17th | FQ2W | 19–22.7 | BV–TV |
| **August 20th** | **FQ15W** | 33.78–36.37 | **V** |
| August 27th | FQ11W | 29.59–32.70 | BV–TV |

The *highlighted* acquisitions are used for estimating the soil-moisture retrieval model constants. Acquisitions are from both morning (descending) and evening (ascending) orbits. Function (as Illustrated in Section III-A2 and Fig. 2): Validation (V), Blind validation (BV), and transfer validation (TV). Validation (V) is performed on scenes used for calibrating/estimating the model constants.

### B. Satellite Data

*1) SAR Data:* Time series of RS2 wide swath fine quad-polarization single-look-complex (SLC) acquisitions covering crop growth cycles (2012 and 2016) was utilized in this investigation, as listed in Table I.

The SLC RS2 data were calibrated, multilooked (Range: 1 and Azimuth: 2 with the resulting range and Azimuth pixel sample spacing of 10.21 m), speckle filtered (boxcar: $3 \times 3$), and range-Doppler terrain corrected (SRTM DEM) to compute co-polarized backscattering coefficients ($\sigma^o_{\mathrm{HH}}$ and $\sigma^o_{\mathrm{VV}}$) employed for the soil moisture retrievals. Incidence angle normalization was introduced as an essential step to bring the SAR acquisitions from different beam modes to a common benchmark (radiometrically comparable), which also extended the domain of validity of the Dubois model ($30^\circ \leq \theta \leq 60^\circ$) [38].

The SLC data (with phase information) were exploited for the generation of polarimetric matrices (coherency and covariance), which were utilized to compute the polarimetric vegetation descriptors for compensating for the vegetation scattering. These matrices were either decomposed or their elements were directly utilized for computing the descriptors. The radar scenes were split between the ones used for estimating the soil moisture retrieval model constants (also used for computing the initial validation RMSE, as highlighted in Table I) and the remaining scenes were utilized for blind and transfer validation. These stages of evaluation are elaborated in Section III-A2 and Fig. 2.

TABLE II
OPTICAL SATELLITE SCENES

| Acquisition Dates (2016) | Sensor |
|---|---|
| May 4th | S2 |
| June 10th | S2 |
| July 18th | L8 |
| August 22nd | S2 |

The availability of such full-polarimetric satellite SAR time series is limited. In this investigation, the number of RS2 scenes was further limited by the fact that, for time-series analysis (and calibration/validation of the retrieval model), the presence of RISMA/U.S. Department of Agriculture (USDA) stations in all the RS2 scenes was a necessary factor. In addition to this, the number of RISMA/USDA stations was reduced due to the unavailability of continuous data as a result of sensor malfunction over some of the agricultural fields. Under such circumstances, it was either not possible to estimate the model constants or perform validation (or both). Our choice of crop types was also limited by these factors and the requirement of common crop types (soya and corn) between the 2016 and 2012 RS2 time series over the test site for demonstrating the transfer of model constants. Therefore, some important crop types, such as wheat and canola, were excluded from this investigation.

*2) Optical Data:* Atmospherically corrected cloud-free Sentinel-2 (S2) and Landsat-8 (L8) surface reflectance scenes, as listed in Table II, were utilized to quantify the crop phenological stages. Only a limited number of cloud-free scenes were available over one of the cropping periods (2016). NDVI, as elaborated in Section III, was utilized to observe the impact of including an optical satellite data-derived vegetation descriptor over the soil moisture retrievals.

### C. In Situ Measurements

The RISMA stations log soil moisture information every 15 min at spatially distinct locations and at varying depths over an agricultural plot. An appropriate timestamp was selected to accurately synchronize the ground-measured soil moisture with the satellite pass time for calibration and validation of the retrieval model. The top layer (0–5 cm) soil moisture was computed as an average of three probes installed at the same depth over different locations to account for the spatial variability within an agricultural plot. The soil texture was measured from soil cores during the installation of the RISMA station network and the crop-type information was provided by the AAFC. In addition to this, the seeding and harvest dates for each station were partially available, as presented in Table III.

The temporarily available USDA soil moisture network with continuous measurements similar to RISMA was used to validate the retrievals from the RS2 time series covering the SMAPVEX'12 period. Each of the SMAPVEX'12 fields was divided into 16 subsites with the USDA station present only over subsite 1. Therefore, subsite 1 allowed for the evaluation of soil moisture retrievals with the transferred model constants (estimated using dedicated scenes from the 2016 RS2 time series). The relative location of the RISMA (2016) and USDA

TABLE III
SMAPVEX (2012) AND RISMA (2016) FIELDS/STATIONS IN CARMAN, MANITOBA, CANADA [35]

| Fields/Stations | Crop Type | Seeding Date | Harvest Date | Sand (%) | Clay (%) |
|---|---|---|---|---|---|
| **52** | Soya | U | U | 52.3 | 29.6 |
| 53 | Corn | U | U | 57.8 | 29.1 |
| 54 | Corn | U | U | 75.1 | 18.6 |
| 63 | Soya | U | U | 86.6 | 9.7 |
| 64 | Soya | U | U | 32.2 | 48.6 |
| 114 | Soya | U | U | 42.4 | 38.6 |
| **MB1** | Soya | May 5th | September 27th | 78.8 | 11.1 |
| MB2 | Peas | U | U | 44.9 | 34.3 |
| MB3 | Corn | U | October 10th | 47.1 | 31.8 |
| MB5 | Soya | May 4th | August 24th | 41.4 | 40.5 |

Soil textures are measured for a depth range of 0–5 cm. U: Unavailable.

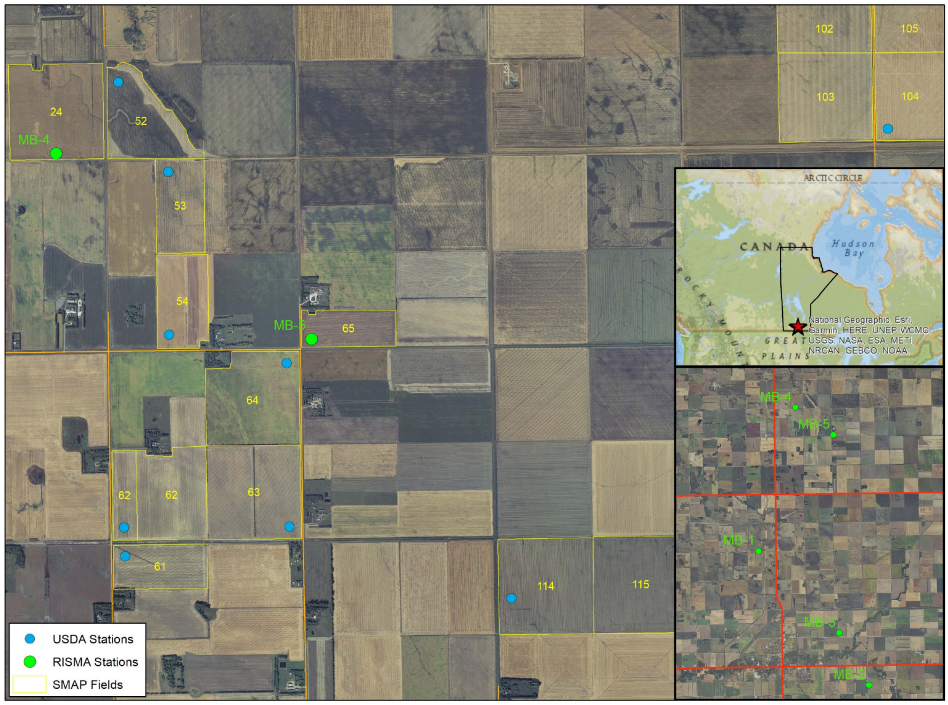


Fig. 1. Relative location of the RISMA (2016) and USDA Stations (SMAPVEX'12), Carman, Manitoba, Canada [39], [40], [41], [42].

TABLE IV
TEMPORAL EVOLUTION OF THE TOTAL CROP BIOMASS (IN $gm^{-2}$) OVER SMAPVEX'12 FIELDS

| | Early June | Early July | Late July |
|---|---|---|---|
| 52 (S) | 131.92 | 1 030.37 | 2 002.20 |
| 53 (C) | 32.97 | 2 757.74 | 3 923.73 |
| 54 (C) | 130.52 | 4 392.39 | 5 836.00 |
| 63 (S) | 86.39 | 624.16 | 1 203.55 |
| 64 (S) | 57.50 | 546.78 | 900.42 |
| 114 (S) | 147.05 | 1 119.38 | 3 274.94 |

S: Soya and C: Corn.

(2012) stations with respect to the SMAPVEX'12 fields can be observed in Fig. 1. The temporal evolution of the total crop biomass (in $gm^{-2}$) over the SMAPVEX'12 fields is presented in Table IV.

Sample size from each crop field varied depending on the number of soil moisture sensors spatially distributed over each field. For fields with three spatially distributed sensors, each sample size consisted around 120 pixels and 30% of this (36 pixels) was used for model calibration. The sample size was kept limited in order to minimize the influence of spatial variability of soil moisture and texture around the RISMA/USDA stations. The pixel sampling was performed within close proximity of each ground station.

### D. Crop Characteristics

Crop characteristics influence the performance of satellite data-derived vegetation descriptors utilized for capturing the plant growth dynamics at different phenological stages, which eventually impacts the performance of soil moisture retrievals. The capability of a satellite SAR sensor to reliably measure

soil moisture through the vegetation volume is effectively determined by the amount of overlying vegetation biomass, the structural attributes of the crop, and the resulting depth of signal penetration at the imaging wavelength. The agricultural fields considered for this investigation were occupied by the following crop types.

*1) Soya:* The soya plant develops as a pair of single blades, which subsequently branches out to mature nodes with compound leaves with three blades. Soil moisture stress in soya-producing regions of the world has been reported to be the principal factor limiting the growth and yield of the crop [43].

*2) Corn:* A well-developed corn plant is often 3 m or taller in height and the spiked ears (female flowers), with the corn kernels encased in sheaths of leaves, develop in the midsection of the plant. While the plant is entering/in the silking stage, it is most sensitive to soil moisture stress that impacts its final yield and its shallow root structure makes it particularly susceptible to droughts [44].

*3) Peas:* Unlike corn, peas are low-growing vines. Severe stress in soil moisture conditions during the postblossom period has been observed to reduce pea yield irrespective of the conditions prevailing prior to blossom [45]. Even though preliminary analysis over a pea field was possible in 2016, further analysis (transfer of the model constants, as elaborated later) was not possible due to the lack of any pea fields during SMAPVEX'12.

## III. Methodology

In contrast to the relatively complex electromagnetic scattering models, such as IEM/AIEM, based on Maxwell's equations, as well as empirical models, such as Oh, the Dubois model allows the dielectric constant to be explicitly expressed as a simple function of the co-polarized backscattering coefficients (HH and VV) and imaging sensor parameters, such as frequency and incidence angle [46], [47]. The preliminary expressions for the Dubois model in terms of the co-polarized backscattering coefficients can be simplified to eliminate the influence of the in situ surface roughness parameter [14]. Furthermore, the effect of correlation length is also inherently absent. The real part of the estimated dielectric constant ($\varepsilon_{\text{est}}$) can then be expressed as

$$\varepsilon_{\text{est}} = \frac{1}{0.024\tan\theta}\log_{10} \times \left(\frac{10^{0.19}\lambda^{0.15}\sigma^{o}{}_{\text{VV:soil}}}{(\cos^{1.82}\theta)(\sin^{0.93}\theta)(\sigma^{o}{}_{\text{HH:soil}})^{0.786}}\right) \quad (1)$$

where $\sigma^{o}{}_{\text{VV:soil}}$ and $\sigma^{o}{}_{\text{HH:soil}}$ are the polarimetric bare soil backscattering coefficients, $\theta$ is the incidence angle, and $\lambda$ is the imaging sensor wavelength ($\lambda = 5.63$ cm for RS2). The SAR scenes were normalized to a common reference angle ($\theta = 37.2^{\circ}$) based on the theoretical cosine relationship of Lambert's law [48] expressed as follows:

$$\sigma^{o}(\theta_{\text{ref}}) = \frac{\cos^2(\theta_{\text{ref}})}{\cos^2(\theta_i)}\sigma^{o}(\theta_i) \quad (2)$$

where $\theta_i$ is the local incidence angle, $\sigma^{o}(\theta_i)$ is the incidence angle-dependent radar backscatter, and $\sigma^{o}(\theta_{\text{ref}})$ is the radar backscatter normalized to the reference incidence angle $\theta_{\text{ref}}$.

In this investigation, we utilized the WCM to parameterize the Dubois model in order to compensate for the vegetation scattering and extend its range of applicability. Even though the original form of the Dubois model was developed for a certain range of volumetric soil moisture content (less than 35% by volume), soil moisture can be estimated beyond this range by considering an appropriate vegetation backscattering model and vegetation descriptors [31]. WCM is a volume scattering model that describes the vegetation canopy as a cloud of water enclosing randomly distributed identical water droplets (vegetative matter) [33]. It is a semi-empirical backscatter model that relates the observed backscattering coefficients to soil backscattering (containing the top layer soil moisture information) and vegetation properties, such as vegetation water content and leaf area index (LAI). Hence, the amalgamation of WCM with a soil moisture retrieval model is crucial for the successful inversion of the latter over vegetated areas. For co-polarized backscattering coefficient ($\sigma^{o}_{pp}$, where $pp =$ HH or VV), the WCM is defined as follows:

$$\sigma^{o}{}_{pp} = \sigma^{o}{}_{\text{veg}} + \tau^2\sigma^{o}{}_{\text{soil}} \quad (3.1)$$

$$\sigma^{o}{}_{\text{veg}} = AV_1\cos\theta_i\left(1-\tau^2\right) \quad (3.2)$$

$$\tau^2 = e^{-2BV_2\sec\theta_i} \quad (3.3)$$

where $V_1$ and $V_2$ are the vegetation descriptors and $A$ and $B$ are the crop-specific model coefficients [31]. Therefore, the observed backscattering ($\sigma^{o}{}_{pp}$) is the sum of the backscattered signal from vegetation volume ($\sigma^{o}_{\text{veg}}$) and bare soil ($\sigma^{o}{}_{\text{soil}}$) modified by the two-way transmittivity of the vegetation ($\tau^2$), which can be expanded and approximated using the Maclaurin series expansion as follows:

$$\tau^2 = e^{-2BV_2\sec\theta_i} = 1 - \frac{2BV_2}{\cos\theta_i} + \frac{1}{2!}\frac{2^2B^2{V_2}^2}{\cos^2\theta_i} - \cdots. \quad (3.4)$$

The expression for $\tau^2$ (and eventually the WCM) is simplified by truncating the series and limiting it to its first two terms. Truncation of the transmittivity term to simplify the WCM is a well-accepted practice adopted by several investigations [31], [42], [49], [50], [51]. Successive inclusion of the higher order terms in the Maclaurin series essentially increases the number of model constants, which makes the process of estimations increasingly challenging and requires more scenes in the time series to participate in the estimation and optimization of the model constants. Considering such aspects, we have adopted the practice of truncating the series to a limited number of terms for the practical implementation of the proposed approach. By truncating the series and retaining only the first two terms, the co-polarized backscattering coefficient ($\sigma^{o}{}_{pp}$) can be expressed as follows:

$$\sigma^{o}{}_{pp} = 2ABV_1V_2 + \left(1 - \frac{2BV_2}{\cos\theta_i}\right)\sigma^{o}{}_{\text{soil}}. \quad (3.5)$$

Therefore, the co-polarized bare soil backscattering coefficient can be expressed as follows:

$$\sigma^{o}{}_{\text{soil}} = \frac{\sigma^{o}{}_{pp} - 2ABV_1V_2}{1 - \frac{2BV_2}{\cos\theta_i}} = \frac{\sigma^{o}{}_{pp} - aV_1V_2}{1 + bV_2} \quad (3.6)$$

$$a = 2AB \quad b = -\frac{2B}{\cos\theta_i}$$

where $a$ and $b$ are the unknown WCM constants (for Dubois–WCM: $a_{\text{HH}}$, $b_{\text{HH}}$, $a_{\text{VV}}$, and $b_{\text{VV}}$ for each agricultural plot) whose accuracy of estimation will essentially determine the soil moisture retrieval accuracy [31]. The bare soil backscattering ($\sigma^o{}_{\text{soil}}$) relationship (3.6) was utilized to parameterize the simplified real dielectric constant expression of the Dubois model. Since the SAR scenes were normalized to a common incidence angle, the incidence angle in (1) is set to $\theta = 37.2°$. For the local incidence angle, $\theta_i$, occurring in the WCM, this information was not utilized since this is only necessary for computing $A$ and $B$, which are the crop-specific model coefficients. For the purpose of retrievals, we utilized the Dubois–WCM constants: $a_{\text{HH}}$, $b_{\text{HH}}$, $a_{\text{VV}}$, and $b_{\text{VV}}$, which are estimated for each agricultural plot.

Although LAI and NDVI have been commonly employed by the past investigations to characterize the phenological state of the vegetation, both are constrained either by the requirement of in situ measurement or the availability of cloud-free optical satellite data, respectively. This reinforces the significance of SAR data-derived vegetation descriptors [42], [52]. In this investigation, we utilized both optical and radar-based polarimetric descriptors. The WCM requires vegetation descriptors in order to account for the impact of vegetation on SAR backscatter. In the past investigations, $V_1$ and $V_2$ were often reduced to a single vegetation descriptor to simplify the WCM [42]. We investigated the performance of soil moisture retrievals by simultaneously combining spectrally unique ($V_1 \neq V_2$) as well as distinct ($V_1 = V_2$) vegetation descriptors (polarimetric and optical) [53]. The idea behind considering the different combinations was to observe the impact of individual as well as the combined effect of simultaneously incorporating spectrally distinct vegetation descriptors over the performance of soil moisture retrievals. The descriptors are elaborated as follows.

*1) NDVI*: Over agricultural fields, NDVI depicts the phenological characteristics and stages of crop growth. The NDVI can, thus, be used as a descriptor of greenery (chlorophyll content) and is expressed as [54] follows:

$$\text{NDVI} = \frac{\text{NIR}_{842\text{ nm}} - \text{RED}_{665\text{ nm}}}{\text{NIR}_{842\text{ nm}} + \text{RED}_{665\text{ nm}}}. \tag{4}$$

The corresponding spectral bands (each optical satellite sensor has a unique band ordering) of the optical satellite sensors (such as Sentinel-2 and Landsat-8) overlapping the NIR (842 nm) and RED (665 nm) wavelengths are utilized for the computation of the NDVI.

*2) Entropy*: The polarimetric entropy is inspired by the information theory of Shannon [55]. As proposed by Cloude and Pottier [56], the full-rank Hermitian positive-semidefinite coherency matrix $\langle[\mathbf{T}]\rangle$ (obtained from the observed polarimetric SAR complex scattering matrix) can be decomposed into three rank 1 coherency matrices $[\mathbf{T}]_i (i = 1, 2, 3)$, which are weighted by their corresponding real positive eigenvalues $\lambda_i$. The normalized eigenvalues

$$p_i = \frac{\lambda_i}{\sum_{i=1}^{3} \lambda_i} \tag{5.1}$$

are the interpretations of the pseudoprobabilities from Shannon's theory, which are used to express the entropy ($H$) as

$$H = -\sum_{i=1}^{3} p_i \log_3 p_i. \tag{5.2}$$

$H$ defines the statistical disorder or the randomness in scattering that occurs as a result of the diversity in the scattering mechanisms within a single resolution cell. Lower values of $H$ indicate the medium to be weakly depolarizing, whereas for higher values of $H$, the scattering cluster is strongly depolarizing in nature.

*3) Radar Vegetation Index (RVI)*: RVI is a well-established SAR data-derived metric for quantifying the evolution of vegetation cover [57]. The index has been employed by investigations, particularly the ones utilizing time-series data, as a measure for monitoring the stage of vegetation growth [58]. The RVI is defined as follows:

$$\text{RVI} = \frac{8\sigma^o_{\text{HV}}}{\sigma^o_{\text{HH}} + \sigma^o_{\text{VV}} + 2\sigma^o_{\text{HV}}} \tag{6}$$

where $\sigma^o_{\text{HV}}$ is the cross-polarized backscattering coefficient and $\sigma^o_{\text{HH}}$ and $\sigma^o_{\text{VV}}$ are the co-polarized backscattering coefficients. The index essentially quantifies the randomness in the radar backscattering, which is formulated by modeling the vegetation canopy as a collection of randomly oriented dipoles. RVI demonstrates an increasing trend, growing from bare field condition to a point in the crop growth cycle where the index is maximum.

*4) Generalized Radar Vegetation Index (GRVI)*: The GRVI was proposed based on the generalized volume scattering model (GVSM). The index is based on the concept of similarity (geodesic distance projected on the unit sphere [59]) between the Kennaugh matrix corresponding to the GVSM ($K_v$) proposed in [60] and the observed Kennaugh matrix ($K$) associated with the PolSAR backscattering from the target [61]. The Kennaugh matrix was introduced by Kennaugh [62] for evaluating the power received in a radar observation. $K_v$ is parameterized by the volume scattering model parameter $\gamma$, which is defined as the co-polarized ratio and can be computed from the elements of the covariance matrix ($\langle[\mathbf{C}]\rangle$). The Kennaugh matrix associated with the target ($K$) can be computed from the elements of the coherency matrix ($\langle[\mathbf{T}]\rangle$). The similarity measure ($f_v$) between $K$ and $K_v$ is computed using the geodesic distance ($\text{GD}_v$), which can be expressed as follows:

$$\text{GD}_v = \text{GD}(K, K_v) \tag{7.1}$$

$$f_v = 1 - \text{GD}_v. \tag{7.2}$$

Another prerequisite for the computation of GRVI is the parameter $\beta$, which is computed as the ratio of the minimum ($p$) to the maximum ($q$) geodesic distance between $K$ and the elementary backscattering targets: trihedral ($K_t$), cylinder ($K_c$), dihedral

($K_d$), and narrow dihedral ($K_{nd}$) [63]

$$\beta = \left(\frac{p}{q}\right)^{2\text{GD}_v} \tag{7.3}$$

$$p = \min \begin{bmatrix} \text{GD}(K, K_t) \\ \text{GD}(K, K_c) \\ \text{GD}(K, K_d) \\ \text{GD}(K, K_{nd}) \end{bmatrix}, \quad q = \max \begin{bmatrix} \text{GD}(K, K_t) \\ \text{GD}(K, K_c) \\ \text{GD}(K, K_d) \\ \text{GD}(K, K_{nd}) \end{bmatrix}.$$

The GRVI is defined as

$$\text{GRVI} = \beta f_v, \quad 0 \leq \text{GRVI} \leq 1. \tag{7.4}$$

With the increase in the fresh crop biomass, the GRVI increases due to an increase in the population of vertical dipole scatterers (for GRVI $= 1, K = K_v$). The GVSM-based GRVI handles ambiguities with regards to scattering mechanisms and correlates better with the biophysical parameters as compared with RVI, which makes it relatively less prone to noise.

### A. Proposed Algorithm

*1) Dubois–WCM Model Constant Estimation:* Selected acquisitions (four scenes) from the RS2 2016 time series were utilized to establish a system of WCM parameterized Dubois equations (four equations for each agricultural plot). Since each agricultural plot had its own set of equations, the solution to the system of equations yielded a unique set of model constants for each plot/crop type (e.g., for MB1: $a_{\text{HH}_{\text{MB1}}}$, $b_{\text{HH}_{\text{MB1}}}$, $a_{\text{VV}_{\text{MB1}}}$, and $b_{\text{VV}_{\text{MB1}}}$). The RS2 acquisitions from 2016 that participated in this process are highlighted in Table I. It is important to understand that since we have considered the simplified form of the Dubois model, the surface roughness information was eliminated from the retrieval process. Furthermore, due to the time-series nature of retrieval of the model constants, the constants captured the variability over the different stages of crop cycle, which is different from estimating them for each individual acquisition (single-scene approach) that requires the presence of sufficient number of fields for each crop type.

Over each agricultural plot (MBs as per Table III), 30% of the randomly selected samples participated in the estimation of the model constants, while the remaining 70% of the samples were reserved for evaluating the goodness of estimation of the model constants. The model constants were calibrated with respect to the in situ soil moisture measurements synchronized with respect to the satellite scene acquisition time. An objective function ($S$)

$$S = \min \sqrt{\frac{1}{n} \sum_{i=1}^{n} |\varepsilon_{\text{obs}i} - \varepsilon_{\text{est}i}|^2} \tag{8}$$

was minimized over several iterations for the determination of optimal set of model constants, where $\varepsilon_{\text{obs}}$ is the observed (9) and $\varepsilon_{\text{est}}$ is the estimated (1) real dielectric constant. $n$ is the number of samples. The Levenberg–Marquardt algorithm was utilized for the optimization of the model constants [64]. The real dielectric constants were obtained using the polynomial dielectric constant model proposed by Hallikainen et al. [65]. The polynomial relates the dielectric behavior of moist soil as a function of soil texture and volumetric soil moisture content ($m_v$) for a range of microwave frequencies. Soil texture has been observed to influence the dielectric behavior over a wide range of frequencies (1.4–18 GHz) and the effect is most pronounced for frequencies below 5 GHz [65]

$$\varepsilon_{\text{obs}} = (a_0 + a_1 S + a_2 C) + (b_0 + b_1 S + b_2 C) m_v + (c_0 + c_1 S + c_2 C) {m_v}^2. \tag{9}$$

In the expression for $\varepsilon_{\text{obs}}$, $S$ and $C$ are the sand and clay percentages, respectively, which constitute the soil texture, as given in Table III, for each agricultural plot (RISMA MB and SMAPVEX'12 stations). For 6 GHz, the coefficient for the real part is $a_0 = 1.993$, $a_1 = 0.002$, $a_2 = 0.015$, $b_0 = 38.086$, $b_1 = -0.176$, $b_2 = -0.633$, $c_0 = 10.720$, $c_1 = 1.256$, and $c_2 = 1.522$.

*2) Performance Assessment:* The goodness of the optimized model constants was evaluated in three different stages: validation (V), blind validation (BV), and transfer validation (TV). The assessment involved the computation of different performance metrics, such as RMSE, Pearson correlation coefficient (PCC), and mean bias error (MBE). The overall PCC and MBE were computed for all possible combinations of the vegetation descriptors utilized during the retrievals.

The following steps were involved in the estimation and evaluation of the model constants (via retrievals), as illustrated in Fig. 2,

*1) Validation (V):* From the RS2 time series, four scenes (from the 2016 acquisitions, as highlighted in Table I) were chosen to estimate the model constants. Over each plot (MBs), the samples were split into two parts, as shown in Fig. 2. While 30% of the randomly selected samples participated in the estimation of the model constant, the remaining 70% of the samples were held out to iteratively test the goodness of the estimation by calculating the validation RMSE. The set of model constants corresponding to the minimum RMSE was finally selected. Therefore, we utilized the 30–70 sample split for optimizing the model constants that led to a minimum validation RMSE.

*2) Blind Validation (BV):* The model constants were then utilized over 100% of the samples over each field from scenes that did not participate in step 1) (non-highlighted acquisitions in Table I). Therefore, this step was termed as blind validation. This stage provided an unbiased evaluation and demonstrated the appropriateness of the estimated model constants for retrievals from the intermediate scenes in the satellite SAR time series.

*3) Transfer Validation (TV):* Since the accuracy of the estimated model constants has been observed to be directly responsible for determining the soil moisture retrieval accuracies [31], we performed transfer validation to confirm this observation. In this step, the model constants from fields with the same crop type (for example, MB1 and MB2 are both soya fields) are exchanged/transferred to observe the impact on the estimated soil moisture. The idea was to observe the range of the soil moisture retrieval errors should such a transfer be deemed necessary. For example, in the absence of any ground measurement over a particular field or the unavailability of suitable satellite time series, the estimation of an optimized set of model constants may not be feasible. Under such circumstances, the transfer of model constants estimated over fields with the same crop type will be

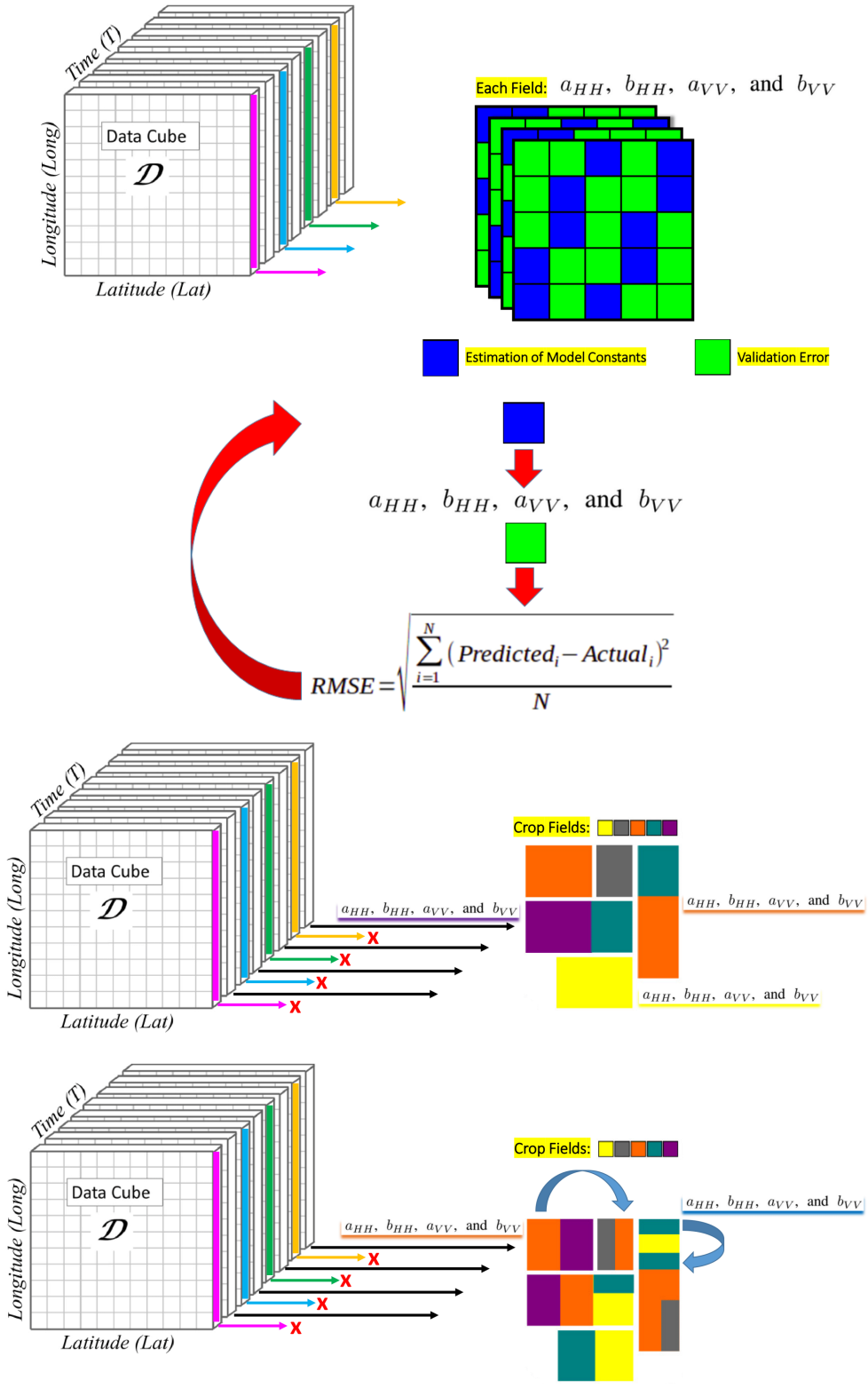


Fig. 2. Schematics for estimation of the model constants and retrieval performance evaluation [53]. Evaluation metrics: validation (V), blind validation (BV), and transfer validation (TV) error. The first data cube (satellite time series) indicates the process of iteratively estimating the model constants using dedicated satellite scenes (colored arrows) from time series spread over the crop growth cycle and validation. The second and third data cube indicates the participation of other scenes (black arrows) in the time series for blind and transfer validation (indicated by the curved blue arrows). Schematic for the Earth observation time-series data cube is modified with permission from Züfle et al. [66].

TABLE V
SOIL MOISTURE ESTIMATION RMSE (IN $m^3$ $m^{-3}$)

| $V_1$=$V_2$ | NDVI | RVI | Entropy | GRVI |
|---|---|---|---|---|
| **Validation** | | | | |
| MB1 | 0.005 6 | 0.003 0 | 0.011 5 | 0.010 0 |
| MB2 | 0.000 9 | 0.001 3 | 0.001 9 | 0.004 3 |
| MB3 | 0.003 3 | 0.004 9 | 0.002 0 | 0.004 7 |
| MB5 | 0.004 4 | 0.003 0 | 0.007 3 | 0.021 8 |
| **Blind Validation** | | | | |
| MB1 | 0.073 4 | 0.060 3 | 0.044 6 | 0.048 4 |
| MB2 | 0.024 1 | 0.025 7 | 0.033 8 | 0.033 4 |
| MB3 | 0.026 0 | 0.028 2 | 0.021 9 | 0.025 3 |
| MB5 | 0.036 0 | 0.039 0 | 0.039 1 | 0.039 9 |
| **Transfer Validation** | | | | |
| MB1 | 0.087 9 | 0.106 3 | 0.106 0 | 0.118 7 |
| MB5 | 0.122 5 | 0.127 3 | 0.133 5 | 0.133 2 |

Polarimetric or optical vegetation descriptor ($V_1$=$V_2$).

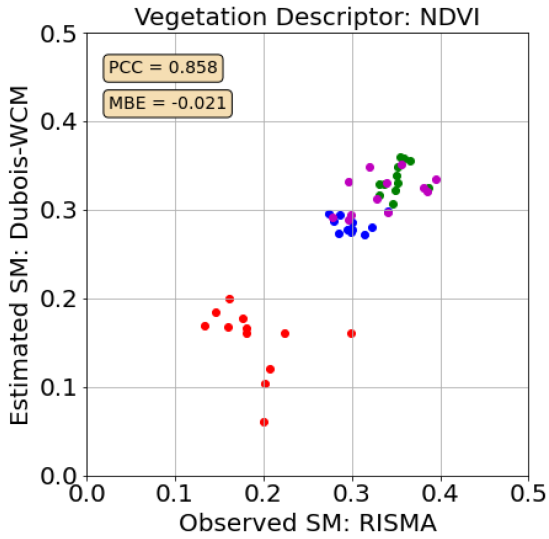


Fig. 3. Blind validation: For optical vegetation descriptor. RISMA Station: MB1: ●, MB2: ●, MB3: ●, and MB5: ●.

helpful. This step revalidated the significance of the uniqueness of the model constants for a particular agricultural plot/crop type.

*3) Choice of Vegetation Descriptors:* The following combination of vegetation descriptors was considered.

*a) Polarimetric or optical vegetation descriptor ($V_1 = V_2$):* In this case, a single polarimetric or optical descriptor was utilized. In the case of the polarimetric descriptors, the issue of temporal latency was absent. On the contrary, for the optical descriptor, the issue of temporal latency was inevitable.

*b) Polarimetric and optical vegetation descriptors ($V_1 \neq V_2$):* In this case, a combination of both polarimetric and optical descriptors was simultaneously utilized. For accommodating the issue of temporal latency, the radar acquisitions were paired with the closest available optical scene.

## IV. RESULTS

### A. Polarimetric or Optical Vegetation Descriptor: $V_1 = V_2$

Table V presents the plotwise soil moisture retrieval RMSEs occurring at different stages of validation, which are obtained using a single vegetation descriptor.

The estimation errors in this stage of validation varied in the range of 0.0009 (over MB2 with NDVI) to 0.0218 (over MB5 with GRVI) $m^3$ $m^{-3}$. The validation performance obtained with the polarimetric descriptors was on par with those obtained with the optical descriptor. There was no clear trend indicating the superiority of the optical over the polarimetric descriptors. Possibly, the temporal latency of the optical scenes impacted this observation.

The blind validation stage offered an unbiased evaluation. The estimation errors in this stage of validation varied in the range of 0.0219 (over MB3 with Entropy) to 0.0734 (over MB1 with NDVI) $m^3$ $m^{-3}$, with MB1 indicating the highest RMSEs. The errors over the peas (MB2) and corn (MB3) fields were relatively lower as compared with the soya fields (MB1 and MB5) for all the descriptors, which varied between 0.0219 and 0.0338 $m^3$ $m^{-3}$. Lower estimation errors indicated better effectiveness of the descriptors for representing the state of the vegetation over the peas and corn fields as compared with the soya fields. The scatter plots between the estimated and the observed soil moisture are presented in Figs. 3 and 4(a), (c), and (e) along with the overall PCC and MBE.

The overall PCC varied in the range of 0.836–0.861, while the overall MBE varied from −0.021 (for NDVI) to 0.003 (for GRVI) $m^3$ $m^{-3}$. Even though the overall PCC remained relatively unchanged, a change in the overall MBE was particularly prominent over MB1 (from negative toward positive) for retrievals with the polarimetric descriptors.

Transfer validation was performed over MB1 and MB5 by exchanging their respective set of model constants. This validation stage highlighted the uniqueness of the model constants for a given agricultural field. Despite the fact that the plots (MB1 and MB5) were both seeded around the same time (May 4th/5th, 2016), they were harvested at different time periods (MB1: September 27th and MB5: August 24th, 2016). The transfer of the model constants from a field at a relatively lagging stage of crop maturation (MB1) to a field at an advanced stage of maturation (MB5) caused a higher rise in the estimation errors. This occurred possibly due to the phenological differences resulting from the different crop growth rates and stages of crop maturation as well as soil moisture conditions. The nuances in the phenological attributes, occurring during the crop growth cycle, are captured by the unique set of model constants. Hence, the model constants estimated over the field at a relatively advanced stage of crop maturation (MB5) captured a more comprehensive picture of the crop growth cycle, which consequently resulted in comparatively better estimation performance over the field that was at a relatively early stage of crop maturation (MB1). Thus, utilizing a set of model constants unique to a particular field is essential for achieving minimal retrieval errors. A comparison of the estimation errors in different stages of validation indicated that the highest retrieval errors occurred during the transfer validation stage, as shown in Fig. 5. The estimation errors in this stage varied in the range of 0.0879–0.1335 (over MB1) $m^3$ $m^{-3}$.

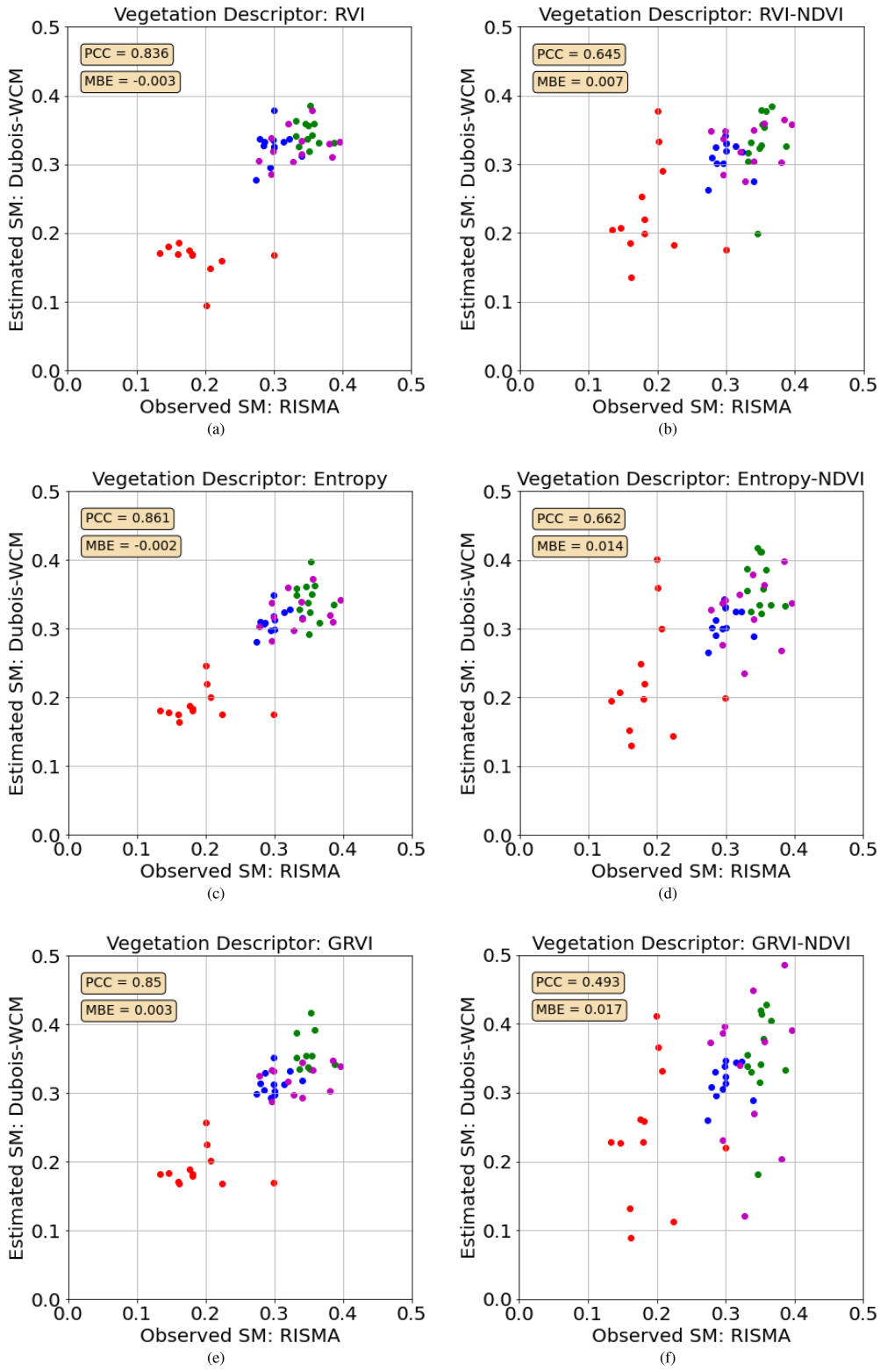


Fig. 4. Blind validation: For polarimetric and polarimetric–optical vegetation descriptors. RISMA Station: MB1: ●, MB2: ●, MB3: ●, and MB5: ●.

We observed RVI to indicate a tendency to saturate on a few occasions and the range of variation for RVI was observed to be relatively smaller as compared with entropy and GRVI. GRVI consistently indicated a wider room for variation by avoiding early saturation and demonstrating continued sensitivity to an extended duration of crop growth, which are desired characteristics of a vegetation descriptor. Some crop types (such as corn, soya, and wheat) indicated relatively better segregation between the range of values for the vegetation descriptors than the others (such as canola). This can possibly be attributed to

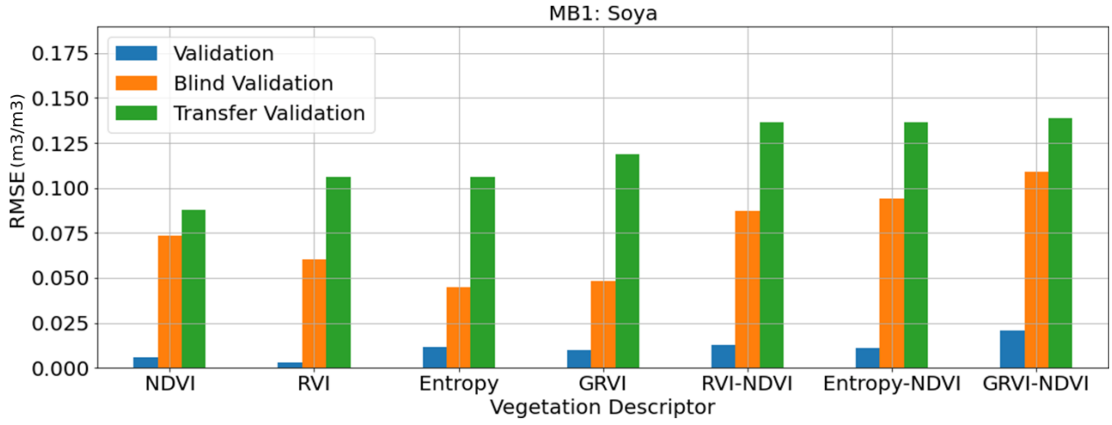


(a)

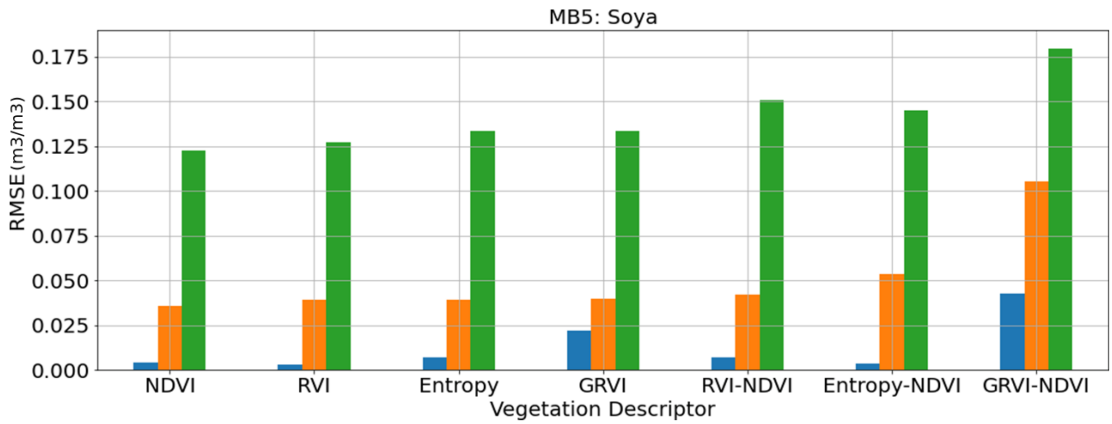


(b)

Fig. 5. Comparison of validation (V), blind validation (BV), and transfer validation (TV) RMSEs (in $m^3\ m^{-3}$).

the prominently discernable structural elements (such as pod and leaf structure) of the crop, which are absent in others.

### B. *Polarimetric and Optical Vegetation Descriptors:* $V_1 \neq V_2$

The impact of introducing the NDVI ($V_2$) in conjunction with the polarimetric descriptors ($V_1$) over the soil moisture retrievals was observed for the same evaluation stages and the errors are presented in Table VI.

Even though the inclusion of the NDVI did improve the validation RMSE over some fields, there was no clear trend to indicate that the combination always resulted in an improvement. Rather, the trend largely indicated an increase in the validation errors. Due to the unavailability of overlapping optical scenes (with RS2 acquisitions), the inability to accurately characterize the spectral information possibly caused the increase in the validation RMSEs. The errors were systematically higher than the errors achieved with a single vegetation descriptor, as presented in Table V.

Relatively higher blind validation RMSEs were observed as compared with the ones obtained with a single descriptor, as shown in Fig. 5. The peas (MB2) and corn (MB3) fields indicated lower errors as compared with the soya fields (MB1 and MB5), which is in agreement with the trend observed in Table V with a single descriptor. The deteriorating effect of incorporating the non-overlapping optical spectral information is evident from the scatter in the plots between the estimated and the observed soil moistures, which is quantified by the decrease in the overall PCC and increase in the overall MBE, as shown in Fig. 4(b), (d),

TABLE VI
SOIL MOISTURE ESTIMATION RMSE (IN $M^3\ M^{-3}$)

| $V_1 \neq V_2$ | RVI-NDVI | Entropy-NDVI | GRVI-NDVI |
|---|---|---|---|
| **Validation** | | | |
| MB1 | 0.012 8 | 0.011 2 | 0.020 5 |
| MB2 | 0.002 4 | 0.002 3 | 0.011 2 |
| MB3 | 0.008 4 | 0.005 2 | 0.007 1 |
| MB5 | 0.006 8 | 0.003 5 | 0.042 5 |
| **Blind Validation** | | | |
| MB1 | 0.087 0 | 0.094 1 | 0.109 0 |
| MB2 | 0.049 2 | 0.042 9 | 0.062 6 |
| MB3 | 0.030 8 | 0.026 0 | 0.031 5 |
| MB5 | 0.041 9 | 0.053 4 | 0.105 3 |
| **Transfer Validation** | | | |
| MB1 | 0.136 5 | 0.136 5 | 0.138 5 |
| MB5 | 0.150 9 | 0.145 2 | 0.179 5 |

Polarimetric and optical vegetation descriptors ($V_1 \neq V_2$).

and (f). The dispersion in the scatter plots is relatively higher over the soya fields (MB1 and MB5) as compared with peas (MB2) and corn (MB3) fields, which explains the superiority in the performance of estimations over the latter. The highest decrease in the overall PCC and the increase in the overall MBE was observed for GRVI–NDVI, where the correlation decreased from 0.85 (GRVI) to 0.493 (GRVI–NDVI) and the bias increased from 0.003 (GRVI) to 0.017 (GRVI–NDVI) $m^3$ $m^{-3}$. This increase in the error possibly occurred due to the combination of mismatching description of the state of vegetation.

The transfer validation errors observed with the combined descriptors were clearly higher than the errors with a single descriptor and varied in the range of 0.1365–0.1795 $m^3$ $m^{-3}$, as shown in Fig. 5. This range represented the highest estimation errors observed in this investigation. The relative relationship between the errors observed over MB1 and MB5 remained the same (errors over MB1 remained lower than MB5), as was observed with a single descriptor.

We observed at least 75% inversion rate for the overall soil moisture retrievals with different combinations of vegetation descriptors. There was no particular preference observed toward any vegetation descriptor or crop type and nearly similar inversion performance was observed for all combinations. A recent investigation by Bhogapurapu et al. [67] with UAVSAR *L*-band data proposed a new vegetation descriptor, which performed better than the conventional optical and polarimetric descriptors. Therefore, the performance of vegetation descriptors may vary according to the imaging wavelength and crop type. Furthermore, higher rates of inversion can possibly be attributed to successful vegetation compensation and incidence angle normalization, which are the factors that may contribute to unstable inversion performance leading to nonphysical results [68]. Although we did not observe a clear trend of decrease in the inversion rates with the progression of crop growth, the retrieval errors for MB1 with relatively lower soil moisture level were indeed higher than the other fields. This observation closely corroborated with the impact of high LAI on soil moisture and total radar backscatter, as presented in [69]. It revealed that under lower soil moisture conditions, the impact of crop volume over the backscattering coefficient was relatively higher, which consequently led to higher estimation errors.

### *C. Transfer Validation Over SMAPVEX'12 RS2 Time Series: With Single Polarimetric Vegetation Descriptor*

We tested the transferability of the model constants over the SMAPVEX'12 fields. The availability of RS2 time series and the temporary USDA soil moisture sensor network enabled the assessment of the performance of model constants estimated from the RS2 time series in 2016. Unlike the 2016 RS2 time series, where the scenes were distributed over the entire cycle from crop emergence to harvest, the scenes in the 2012 time series were concentrated around a limited period of the cropping cycle. This exercise demonstrated retrievals under data-constrained conditions when obtaining an optimized set of model constants was not feasible due to the concentrated nature of the scenes. In order to enable the transfer of the model constants, SMAPVEX'12 fields with common crop types (MB5: soya fields and MB3: corn fields) were selected.

The soil moisture retrievals can be observed in Fig. 6, presented alongside the continuous measurement of ground-based soil moisture at the USDA stations. The estimated soil moisture over the fields closely followed the USDA station measurements until the soil moisture dropped below a critical level. It is interesting to note that, while the retrievals over both the corn fields (53 and 54) indicated consistent overestimation, the soil moisture over the soya fields was underestimated under high soil moisture conditions and overestimated for some drying fields. Furthermore, the overestimation was slightly higher for the relatively drier corn field (53). It is noteworthy that the retrievals captured the fine variations in the soil moisture condition between the morning (higher moisture) and evening (lower moisture) acquisitions, as highlighted in Fig. 6. The observed transfer validation RMSEs over the SMAPVEX'12 fields were in a similar range, as observed in Tables V and VI.

Toward the end of June 12, the moisture over the fields steadily decreased indicating an overall drying tendency (see Fig. 6). The time series of the polarimetric vegetation descriptors, as shown in Fig. 7, exhibited a consistently increasing trend during the SMAPVEX'12 time period (from June 5th to July 13th, 2012), which was in agreement with the field measured total crop biomass information, as presented in Table IV. As the soil moisture decreased and crop volume increased, the error in retrievals increased, particularly over the corn fields (53 and 54).

It is interesting that the field measurements, as presented in Table IV, revealed that, among all the fields, the corn fields had the highest volume of total crop biomass. This observation was consistent with the backscatter/volumetric soil moisture–LAI relationship presented in [69] and the decorrelation reported in [70] between the TerraSAR-X backscattering and surface soil moisture over corn fields at advanced growth stages. The vegetation descriptors (computed from the same day ascending and descending acquisitions) indicated a noticeable diurnal change. Early morning acquisitions indicated lower values of the descriptors for nearly a similar state of crop volume, a trend that was observed to be consistent with all the polarimetric descriptors. This intraday variation can be justified by the observations from [71], where the radar backscatter was reported to be influenced by dew and intercepted precipitation settled over the agricultural vegetation. In our investigation, at *C*-band, such variations can be linked to the diurnal change in the surface soil moisture conditions between the two satellite acquisitions.

We observed a diverse range of retrieval performance over the SMAPVEX'12 fields, as presented in Table VII. Due to the nature of the retrievals (via transfer of the model constants), an increase in the retrieval errors was expected. Although the model constants were estimated for the same crop types (grown in 2016), the constants sensitive to the crop characteristics probably lacked some information due to differing growing conditions or perhaps due to a different variant of the same crop type. Therefore, depending on the similarity between the crop growth conditions in 2016 (native fields) and 2012 (fields where the constants were transferred), the proximity of the retrievals to

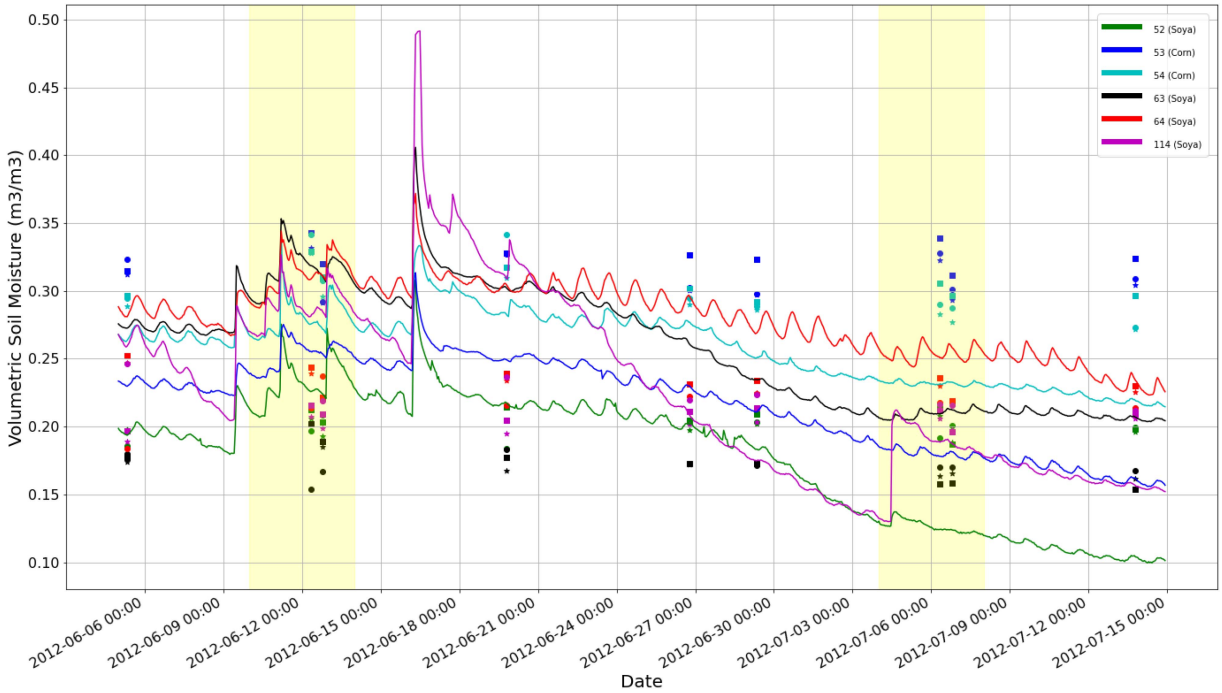


Fig. 6. Soil moisture retrievals around SMAPVEX'12 USDA stations with transfer of model constants. Polarimetric vegetation descriptors: RVI: ●, Entropy: ∗, and GRVI: ■. Highlighted: morning (descending) and evening (ascending) RS2 acquisitions for June 12th and July 6th, 2012. The solid lines indicate the continuous soil moisture measurements from the USDA stations.

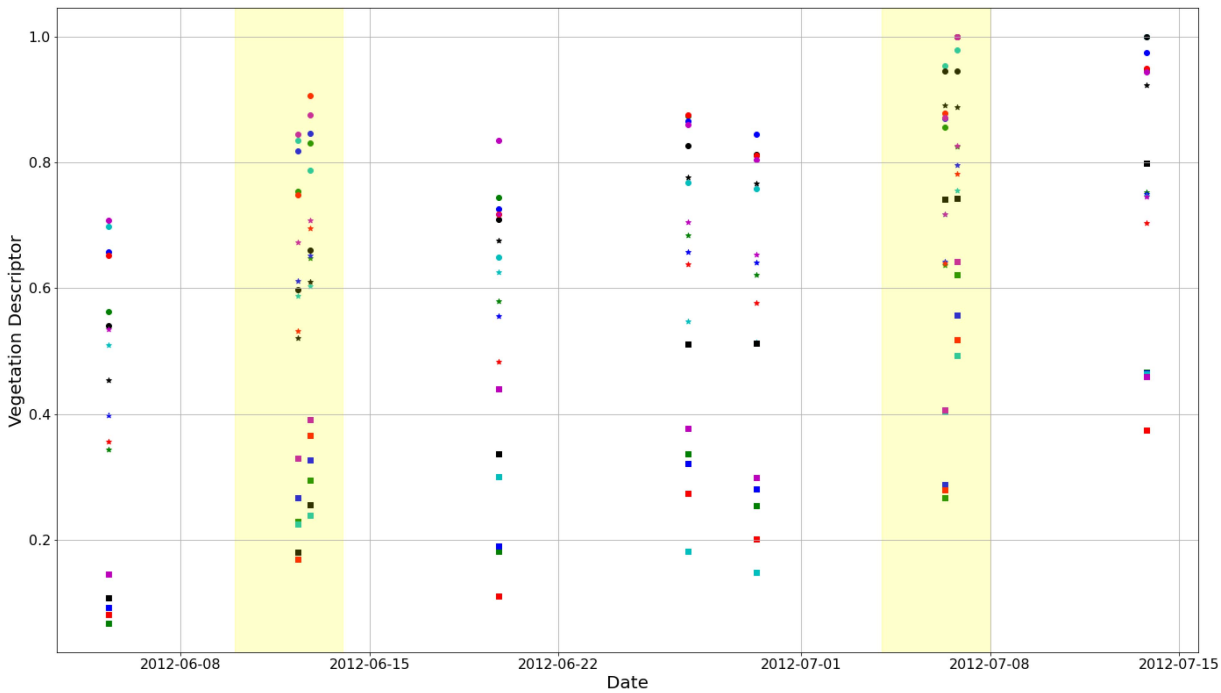


Fig. 7. Time series of polarimetric vegetation descriptors over SMAPVEX'12 fields. Polarimetric vegetation descriptors: RVI: ●, Entropy: ∗, and GRVI: ■. Colors differentiate the SMAPVEX'12 fields, as per Fig. 6.

the actual ground conditions varied [72]. In addition to this contributing to the deviation, the crop volume also obscured the surface soil moisture information from the radar signal. Under such a situation, a certain level (higher than a threshold) of soil moisture can perhaps provide some compensation for the obscuring effect of vegetation, which may consequently result in better matching between the ground measurements and satellite observations. Fig. 6 indicated better retrieval performance during the relatively lower crop biomass period as compared with the relatively denser vegetation period.

TABLE VII
FIELDWISE PERFORMANCE OF SOIL MOISTURE ESTIMATION (IN $m^3$ $m^{-3}$) WITH TRANSFER OF MODEL CONSTANTS ESTIMATED WITH POLARIMETRIC VEGETATION DESCRIPTORS ($V_1 = V_2$): FOR SMAPVEX'12 RS2 TIME SERIES

| $V_1$=$V_2$ | RVI | Entropy | GRVI |
|---|---|---|---|
| **Transfer Validation** | | | |
| **52 (S)** | | | |
| RMSE | 0.049 7 | 0.048 9 | 0.049 7 |
| PCC | −0.038 1 | 0.234 0 | 0.450 4 |
| MBE | 0.019 3 | 0.021 8 | 0.027 0 |
| **53 (C)** | | | |
| RMSE | 0.102 8 | 0.097 2 | 0.113 8 |
| PCC | 0.198 0 | 0.194 3 | 0.171 9 |
| MBE | 0.097 0 | 0.091 2 | 0.108 8 |
| **54 (C)** | | | |
| RMSE | 0.048 5 | 0.038 8 | 0.052 3 |
| PCC | 0.768 6 | 0.778 6 | 0.584 1 |
| MBE | 0.046 1 | 0.036 2 | 0.049 1 |
| **63 (S)** | | | |
| RMSE | 0.098 4 | 0.091 4 | 0.090 1 |
| PCC | −0.106 3 | 0.769 6 | 0.932 2 |
| MBE | −0.088 0 | −0.084 8 | −0.085 2 |
| **64 (S)** | | | |
| RMSE | 0.068 4 | 0.058 7 | 0.052 1 |
| PCC | 0.180 4 | 0.047 4 | 0.203 9 |
| MBE | −0.062 7 | −0.051 5 | −0.045 1 |
| **114 (S)** | | | |
| RMSE | 0.048 6 | 0.061 9 | 0.057 6 |
| PCC | 0.510 0 | −0.444 2 | −0.093 1 |
| MBE | −0.005 0 | −0.027 1 | −0.020 2 |

S: Soya and C: Corn.

Under increasing LAI conditions, the obscuring effect of the vegetation becomes prominent enough to not allow the soil moisture information to impact the total radar backscatter, which may occur at relatively lower LAIs for shorter imaging wavelengths. Past Earth observation investigations have reported such obscuring action of the overlying vegetation to land cover signature at microwave and optical frequencies [12], [73]. Degradation in the performance of the retrievals under high crop biomass (along with low soil moisture) conditions may impact the overall PCC, which may apparently make the retrieval approach appear like a weakly performing one. However, it is important to realize that the performance of retrievals is not solely determined by the accuracy of empirical/semi-empirical models or even the effectiveness of the vegetation compensation model. Rather, it may be limited by the feasibility of information that can be captured by the satellite sensor under vegetation obscuring conditions [73]. Some recent investigations have highlighted the role of data distribution (influenced by the stage of crop maturity) and statistical measures, such as skewness (indicates the dominance of the scattering mechanisms), for agricultural applications with SAR data [74]. Such factors may also influence the performance of soil moisture retrievals while transferring a model and determine the extent of generalization of a model [75].

## V. DISCUSSION

With the single-scene approach, the solution to the WCM-compensated Dubois model would require at least four crop fields for each crop type to solve for the four model constants ($a_{HH}$, $b_{HH}$, $a_{VV}$, and $b_{VV}$ estimated for each agricultural plot for model calibration). Certain datasets, such as ours, do not support this requirement due to limited fields available for each crop type. This limitation exactly served as the motivation for the proposed time-series approach that instead exploited the temporal dimension of the satellite data. This essentially resolved the issue of limited crop fields in a single scene for estimating the model constants. Furthermore, it accounted for capturing the crop phenology present in the satellite scenes distributed over the time series, which would have, otherwise, been missing in the case of single-scene model calibration. Some investigations, such as [31], have reported the model constants, while others, such as [42], have only reported the performance in terms of the retrieval results. The values of such constants are not absolute but rather sensitive to the change in the sensor configuration, pattern of crop growth phenology, crop variant, etc.

Through the proposed time-series model calibration approach that required incidence angle normalization of the SAR scenes, we also addressed the issue of incidence angle dependence of the soil moisture retrieval accuracies, as reported by Bai and He [31]. Since we utilized the simplified form of the Dubois model, the surface roughness term was eliminated from the expression and the dielectric constant was expressed as a simplified function of the co-polarized backscattering coefficients and sensor configuration parameters. Since the simplified Dubois model was employed in our investigation for its ease of inversion, we have not presented/utilized any surface roughness information. It is possible that the inclusion of the roughness information may further improve the performance of retrievals. However, the acquisition of such information is not only challenging due to the manual efforts involved but it is also impractical for operational monitoring of soil moisture and infeasible (not possible without destructing the crops) to measure at advanced stages of crop growth. Moreover, even if such information is available during the advanced stages of crop growth, it is difficult to segregate the contributions of the soil surface roughness and the randomness in scattering offered by the crop biomass to the radar backscatter offered by the crop biomass to the radar backscatter. Therefore, we believe that although the inclusion of the surface roughness information may not change the final conclusion of this investigation, it may probably impact the accuracy/performance of the retrieved soil moisture.

The results from the proposed time-series approach closely met the observational requirements in terms of soil moisture retrieval accuracy ($\leq 5\%$ in volume) and spatial resolution ($\leq$ 1 km), as defined by the global monitoring for environment and security services [22], [24]. Our approach considered the classical semi-empirical WCM for vegetation compensation that merged well with the Dubois model to achieve the 0.04 $m^3$ $m^{-3}$ RMSE benchmark at a high spatial resolution. Xing et al. [76] also reported better retrieval accuracies (4.3 vol.%) over wheat and soya fields during the growing season by coupling the

Dubois model with a modified WCM. Although such soil moisture retrieval accuracies have been demonstrated over bare or sparsely vegetated agricultural areas with SAR sensors operating at *L*, *C*, and *X*-band, the performance of retrievals observed in our investigation with *C*-band at high spatial resolution have been seldom reported over vegetated areas during a crop growth cycle [77], [78]. In addition to this, our time-series approach also addressed the issue of estimating the Dubois–WCM model constants under data-constrained conditions when only a limited number of fields (less than the number of model constants) are available per crop type with corresponding ground measurements. We implemented the WCM-compensated Dubois model in a time-series manner, which was inspired by investigations that exploited the strength of multitemporality of the SAR datasets for obtaining a better estimate of the biophysical parameters and soil moisture [79], [80].

In order to compensate for scattering from growing crop volume, the effectiveness of the optical and polarimetric descriptors was tested individually as well as in a combined manner. Our investigation demonstrated the crucial role of a single polarimetric descriptor in solely compensating for the vegetation scattering. With a single descriptor, the blind validation RMSEs varied in the range of 0.0219–0.0734 $m^3\ m^{-3}$, which fell in close proximity to the accepted 0.04 $m^3\ m^{-3}$ RMSE benchmark of the passive soil moisture missions. Furthermore, the estimation errors for peas and corn remained below this benchmark, varying between 0.0219 and 0.0399 $m^3\ m^{-3}$. Li and Wang [42] utilized polarimetric and optical vegetation descriptors in the WCM for soil moisture retrieval from RS2 time series covering SMAPVEX'12 over the Manitoba site (as considered in our investigation) and reported retrieval RMSEs of 0.069, 0.085, and 0.071 $m^3\ m^{-3}$ for $\sigma^o{}_{\mathrm{HV}}$, RVI, and NDVI (utilized as vegetation descriptors), respectively.

We observed that when the non-overlapping radar and optical descriptors were combined, it resulted in an increase in the estimation errors with a decrease in the overall PCCs and an increase in the overall MBEs. This indicated that it was perhaps the combination of the incoherent/mismatching vegetation description rather than solely the temporal latency of the optical scenes that was causing the degradation in the performance. The overall PCCs observed with both the optical and polarimetric descriptors varied in the range of 0.836–0.861. Temporal latency indicated a higher sensitivity toward the overall MBE as compared with the overall PCC.

We demonstrated that the lack of *a priori* knowledge of the surface roughness information during soil moisture retrievals can be partially addressed by employing the simplified Dubois model. However, the true significance and sensitivity of the surface roughness over the retrievals can only be reliably assessed by actually performing the retrievals with and without the roughness information and, subsequently, observing the impact on the performance metrics. Considering the simplified Dubois model retrieval methodology (without any requirement for roughness information) adopted in this investigation, we have not indulged in the discussion over the impact of surface roughness on the quality of retrievals or attempted to correlate the differences in the roughness between the agricultural fields with poor transfer validation performance, which was observed over some fields. Apart from the vegetation descriptors, the WCM constants ($a_{\mathrm{HH}}$, $b_{\mathrm{HH}}$, $a_{\mathrm{VV}}$, and $b_{\mathrm{VV}}$) do not explicitly provide a way to include a roughness term. Nevertheless, since the field roughness is coupled to the radar backscatter, its impact may be inherently present in these constants. Therefore, the transfer of these constants to a field with different roughness profiles may be one of the reasons for the rise in the transfer validation error. A detailed field campaign over the agricultural test site with synchronized acquisition of satellite time series is necessary to reliably establish such correlations.

## VI. Conclusion

The following key observations can be concluded from this investigation.

1) We estimated the Dubois–WCM model constants using scenes (located at different phenological stages) selected from a satellite SAR time series covering a crop growth cycle. This time-series manner of model calibration enabled us to capture the phenological nuances occurring at different stages of crop growth over an agricultural plot.
2) Our investigation presented notable performance of soil moisture retrievals with single optical and polarimetric vegetation descriptor ($V_1 = V_2$). However, our results did not reveal a preference toward any particular descriptor. Rather, the performance of the retrievals with the single optical or polarimetric vegetation descriptor was observed to be nearly similar. Furthermore, we demonstrated that a combination of temporally non-overlapping vegetation descriptors ($V_1 \neq V_2$) resulted in degradation in the performance of the retrievals. Therefore, it remains to be investigated if a combination of perfectly overlapping optical and polarimetric vegetation descriptors (with no temporal latency) can indeed improve the performance beyond those obtained with a single descriptor.
3) Transfer validation of the model constants between agricultural fields with the same crop type indicated that constants estimated over fields at a relatively advanced stage of crop maturation performed better than those estimated over fields at a relatively earlier stage. Such a set of model constants (estimated over the fields at a relatively advanced stage) encapsulated a more comprehensive picture of the crop phenological cycle. We observed that the transfer of such constants consequently led to lower transfer validation errors. This exercise also provided an idea regarding the tolerance of the performance metrics (RMSE, PCC, and MBE) of retrievals that one can expect with such a transfer. In case of such a transfer, the performance of retrievals will depend on the similarity in the crop growth conditions between the native field (where the constants were estimated) and the target field (where the constants are transferred). In case of absence/malfunctioning of ground instrumentation over an agricultural field, retrievals with a set of transferred model constants will be crucial to obtain an estimate of the prevailing state of soil moisture (dry/wet).

## ACKNOWLEDGMENT

The authors would like to thank the Canadian Space Agency for the satellite SAR time series, AAFC, ECCC, and USDA for their efforts for the in situ measurements, K. Gottfried, J. Powers, A. Halstead, and H. McNairn from AAFC, R. Touzi (Canada Centre for Remote Sensing), A. Berg (University of Guelph, Canada), J. Li (Natural Resources Canada), S. Shirtliffe (University of Saskatchewan, Canada), M. Cosh (USDA-Agricultural Research Service, USA), X. Bai (NUIST, China), A. Bhattacharya (MRSL, IIT Bombay, India), A. C. Frery (Victoria University of Wellington, New Zealand), N. Oppelt (EOM, CAU Kiel, Germany), A. Züfle (Emory University, USA), Saeid Homayouni (Eau Terre Environnement Research Centre, INRS, Québec, Canada), Kiel Marine Science (KMS) and B. S. Daya Sagar (ISI Bangalore, India) for their kind support and insightful discussions, and the anonymous reviewers for their critical and constructive comments.

## REFERENCES

[1] D. L. Spittlehouse and R. B. Stewart, "Adaptation to climate change in forest management," *Ann. Forest Sci.*, vol. 72, pp. 145–167, 2003.

[2] Y. H. Kerr et al., "The SMOS mission: New tool for monitoring key elements of the global water cycle," *Proc. IEEE*, vol. 98, no. 5, pp. 666–687, May 2010.

[3] D. Entekhabi et al., "The soil moisture active passive (SMAP) mission," *Proc. IEEE*, vol. 98, no. 5, pp. 704–716, May 2010.

[4] A. Balenzano et al., "Sentinel-1 soil moisture at 1 km resolution: A validation study," *Remote Sens. Environ.*, vol. 263, 2021, Art. no. 112554.

[5] M. Khazaei, S. Hamzeh, N. N. Samani, A. Muhuri, K. Goïta, and Q. Weng, "A web-based system for satellite-based high-resolution global soil moisture maps," *Comput. Geosci.*, vol. 170, 2023, Art. no. 105250.

[6] E. Santi, S. Paloscia, S. Pettinato, L. Brocca, L. Ciabatta, and D. Entekhabi, "On the synergy of SMAP, AMSR2 AND SENTINEL-1 for retrieving soil moisture," *Int. J. Appl. Earth Observ. Geoinf.*, vol. 65, pp. 114–123, 2018.

[7] B. Bauer-Marschallinger et al., "Toward global soil moisture monitoring with Sentinel-1: Harnessing assets and overcoming obstacles," *IEEE Trans. Geosci. Remote Sens.*, vol. 57, no. 1, pp. 520–539, Jan. 2019.

[8] L. Pulvirenti et al., "A surface soil moisture mapping service at National (Italian) scale based on Sentinel-1 data," *Environ. Model. Softw.*, vol. 102, pp. 13–28, 2018.

[9] N. Pierdicca, L. Pulvirenti, and C. Bignami, "Soil moisture estimation over vegetated terrains using multitemporal remote sensing data," *Remote Sens. Environ.*, vol. 114, no. 2, pp. 440–448, 2010.

[10] N. Pierdicca, L. Pulvirenti, and G. Pace, "A prototype software package to retrieve soil moisture from Sentinel-1 data by using a Bayesian multitemporal algorithm," *IEEE J. Sel. Topics Appl. Earth Observ. Remote Sens.*, vol. 7, no. 1, pp. 153–166, Jan. 2014.

[11] F. Mattia, G. Satalino, V. Pauwels, and A. Loew, "Soil moisture retrieval through a merging of multi-temporal l-band SAR data and hydrologic modelling," *Hydrol. Earth Syst. Sci.*, vol. 13, no. 3, pp. 343–356, 2009.

[12] A. Balenzano, F. Mattia, G. Satalino, and M. W. Davidson, "Dense temporal series of C-and L-band SAR data for soil moisture retrieval over agricultural crops," *IEEE J. Sel. Topics Appl. Earth Observ. Remote Sens.*, vol. 4, no. 2, pp. 439–450, Jun. 2011.

[13] L. Zhu, R. Si, X. Shen, and J. P. Walker, "An advanced change detection method for time-series soil moisture retrieval from Sentinel-1," *Remote Sens. Environ.*, vol. 279, 2022, Art. no. 113137.

[14] A. Merzouki, H. McNairn, and A. Pacheco, "Mapping soil moisture using RADARSAT-2 data and local autocorrelation statistics," *IEEE J. Sel. Topics Appl. Earth Observ. Remote Sens.*, vol. 4, no. 1, pp. 128–137, Mar. 2011.

[15] H. Lievens and N. E. Verhoest, "Spatial and temporal soil moisture estimation from RADARSAT-2 imagery over Flevoland, The Netherlands," *J. Hydrol.*, vol. 456, pp. 44–56, 2012.

[16] M. Trudel, F. Charbonneau, and R. Leconte, "Using RADARSAT-2 polarimetric and ENVISAT-ASAR dual-polarization data for estimating soil moisture over agricultural fields," *Can. J. Remote Sens.*, vol. 38, no. 4, pp. 514–527, 2012.

[17] M. Choker et al., "Evaluation of the OH, Dubois and IEM backscatter models using a large dataset of SAR data and experimental soil measurements," *Water*, vol. 9, no. 1, 2017, Art. no. 38.

[18] L. Chen et al., "Estimating soil moisture over winter wheat fields during growing season using machine-learning methods," *IEEE J. Sel. Topics Appl. Earth Observ. Remote Sens.*, vol. 14, pp. 3706–3718, Mar. 2021.

[19] L. Pasolli et al., "Polarimetric radarsat-2 imagery for soil moisture retrieval in Alpine areas," *Can. J. Remote Sens.*, vol. 37, no. 5, pp. 535–547, 2011.

[20] E. Santi, M. Dabboor, S. Pettinato, and S. Paloscia, "Combining machine learning and compact polarimetry for estimating soil moisture from C-band SAR data," *Remote Sens.*, vol. 11, no. 20, 2019, Art. no. 2451.

[21] E. Santi, S. Paloscia, S. Pettinato, and G. Fontanelli, "Application of artificial neural networks for the soil moisture retrieval from active and passive microwave spaceborne sensors," *Int. J. Appl. Earth Observ. Geoinf.*, vol. 48, pp. 61–73, 2016.

[22] S. Paloscia, S. Pettinato, E. Santi, C. Notarnicola, L. Pasolli, and A. Reppucci, "Soil moisture mapping using Sentinel-1 images: Algorithm and preliminary validation," *Remote Sens. Environ.*, vol. 134, pp. 234–248, 2013.

[23] C. Notarnicola, M. Angiulli, and F. Posa, "Soil moisture retrieval from remotely sensed data: Neural network approach versus Bayesian method," *IEEE Trans. Geosci. Remote Sens.*, vol. 46, no. 2, pp. 547–557, Feb. 2008.

[24] E. Santi, S. Paloscia, S. Pettinato, C. Notarnicola, L. Pasolli, and A. Pistocchi, "Comparison between SAR soil moisture estimates and hydrological model simulations over the Scrivia test site," *Remote Sens.*, vol. 5, no. 10, pp. 4961–4976, 2013.

[25] J. Ezzahar et al., "Evaluation of backscattering models and support vector machine for the retrieval of bare soil moisture from Sentinel-1 data," *Remote Sens.*, vol. 12, no. 1, 2020, Art. no. 72.

[26] P.K. Srivastava, G. Petropoulos, and Y. H. Kerr, *Satellite Soil Moisture Retrieval: Techniques and Applications*. Amsterdam, The Netherlands: Elsevier, 2016.

[27] L. Karthikeyan, M. Pan, N. Wanders, D. N. Kumar, and E. F. Wood, "Four decades of microwave satellite soil moisture observations: Part 1—A review of retrieval algorithms," *Adv. Water Resour.*, vol. 109, pp. 106–120, 2017.

[28] S. C. Steele-Dunne, H. McNairn, A. Monsivais-Huertero, J. Judge, P.-W. Liu, and K. Papathanassiou, "Radar remote sensing of agricultural canopies: A review," *IEEE J. Sel. Topics Appl. Earth Observ. Remote Sens.*, vol. 10, no. 5, pp. 2249–2273, May 2017.

[29] M. Callens, N. E. Verhoest, and M. W. Davidson, "Parameterization of tillage-induced single-scale soil roughness from 4-m profiles," *IEEE Trans. Geosci. Remote Sens.*, vol. 44, no. 4, pp. 878–888, Apr. 2006.

[30] N. E. Verhoest, H. Lievens, W. Wagner, J. Álvarez-Mozos, M. S. Moran, and F. Mattia, "On the soil roughness parameterization problem in soil moisture retrieval of bare surfaces from synthetic aperture radar," *Sensors*, vol. 8, no. 7, pp. 4213–4248, 2008.

[31] X. Bai and B. He, "Potential of Dubois model for soil moisture retrieval in prairie areas using SAR and optical data," *Int. J. Remote Sens.*, vol. 36, no. 22, pp. 5737–5753, 2015.

[32] P. C. Dubois, J. van Zyl, and T. Engman, "Measuring soil moisture with imaging radars," *IEEE Trans. Geosci. Remote Sens.*, vol. 33, no. 4, pp. 915–926, Jul. 1995.

[33] E. Attema and F. T. Ulaby, "Vegetation modeled as a water cloud," *Radio Sci.*, vol. 13, no. 2, pp. 357–364, 1978.

[34] F. C. Kahimba, R. S. Ranjan, J. Froese, M. Entz, and R. Nason, "Cover crop effects on infiltration, soil temperature, and soil moisture distribution in the Canadian prairies," *Appl. Eng. Agriculture*, vol. 24, no. 3, pp. 321–333, 2008.

[35] A. Pacheco et al., "Real-time in-situ soil monitoring for agriculture (RISMA) network metadata," in *Science and Technology Branch Agriculture and Agri-Food Canada*, 2019.

[36] H. A. Bhuiyan et al., "Assessing SMAP soil moisture scaling and retrieval in the Carman (Canada) study site," *Vadose Zone J.*, vol. 17, no. 1, pp. 1–14, 2018.

[37] A. Merzouki, H. McNairn, J. Powers, and M. Friesen, "Synthetic aperture radar (SAR) compact polarimetry for soil moisture retrieval," *Remote Sens.*, vol. 11, no. 19, 2019, Art. no. 2227.

[38] V. Zyl and Y. Kim, *Synthetic Aperture Radar Polarimetry*. Hoboken, NJ, USA: Wiley, 2011.

[39] H. McNairn et al., "The soil moisture active passive validation experiment 2012 (SMAPVEX12): Prelaunch calibration and validation of the SMAP soil moisture algorithms," *IEEE Trans. Geosci. Remote Sens.*, vol. 53, no. 5, pp. 2784–2801, May 2015.

[40] E. R. Ojo, P. R. Bullock, J. L'Heureux, J. Powers, H. McNairn, and A. Pacheco, "Calibration and evaluation of a frequency domain reflectometry sensor for real-time soil moisture monitoring," *Vadose Zone J.*, vol. 14, no. 3, pp. 1–12, 2015.

[41] D. Clewley et al., "A method for upscaling in situ soil moisture measurements to satellite footprint scale using random forests," *IEEE J. Sel. Topics Appl. Earth Observ. Remote Sens.*, vol. 10, no. 6, pp. 2663–2673, Jun. 2017.

[42] J. Li and S. Wang, "Using SAR-derived vegetation descriptors in a water cloud model to improve soil moisture retrieval," *Remote Sens.*, vol. 10, no. 9, 2018, Art. no. 1370.

[43] E. Brown, C. Caviness, and D. Brown, "Response of selected soybean cultivars to soil moisture deficit 1," *Agron. J.*, vol. 77, no. 2, pp. 274–278, 1985.

[44] O. Denmead and R. H. Shaw, "The effects of soil moisture stress at different stages of growth on the development and yield of corn 1," *Agron. J.*, vol. 52, no. 5, pp. 272–274, 1960.

[45] A. Maurer, H. Fletcher, and D. Ormrod, "Response of peas to environment: IV—Effect of five soil water regimes on growth and development of peas," *Can. J. Plant Sci.*, vol. 48, no. 2, pp. 129–137, 1968.

[46] Y. Oh, K. Sarabandi, and F. T. Ulaby, "An empirical model and an inversion technique for radar scattering from bare soil surfaces," *IEEE Trans. Geosci. Remote Sens.*, vol. 30, no. 2, pp. 370–381, Mar. 1992.

[47] A. K. Fung, *Microwave Scattering and Emission Models and Their Applications*. Norwood, MA, USA: Artech House, 1994.

[48] F. T. Ulaby, "Microwave remote sensing active and passive," in *Rader Remote Sensing and Surface Scattering and Emission Theory*. New York, NY, USA: Longman Higher Education, 1982, pp. 848–902.

[49] M. Kseneman and D. Gleich, "Soil moisture estimation from X-band data using Tikhonov regularization and neural net," *IEEE Trans. Geosci. Remote Sens.*, vol. 51, no. 7, pp. 3885–3898, Jul. 2013.

[50] Y. Bao, L. Lin, S. Wu, K. A. K. Deng, and G. P. Petropoulos, "Surface soil moisture retrievals over partially vegetated areas from the synergy of Sentinel-1 and Landsat 8 data using a modified water-cloud model," *Int. J. Appl. Earth Observ. Geoinf.*, vol. 72, pp. 76–85, 2018.

[51] M. Mardan and S. Ahmadi, "Soil moisture retrieval over agricultural fields through integration of synthetic aperture radar and optical images," *GISci. Remote Sens.*, vol. 58, no. 8, pp. 1276–1299, 2021.

[52] H. Wang, R. Magagi, K. Goïta, Y. Duguay, M. Trudel, and A. Muhuri, "Retrieval performances of different crop growth descriptors from full- and compact-polarimetric SAR decompositions," *Remote Sens. Environ.*, vol. 285, 2023, Art. no. 113381.

[53] A. Muhuri, K. Goïta, R. Magagi, and H. Wang, "Exploiting satellite SAR time-series for soil moisture retrieval during crop growth cycle," in *Proc. 10th Int. Conf. Agro-Geomatics; 43rd Can. Symp. Remote Sens.*, 2022, pp. 1–2.

[54] C. J. Tucker, "Red and photographic infrared linear combinations for monitoring vegetation," *Remote Sens. Environ.*, vol. 8, pp. 127–150, 1979.

[55] C. E. Shannon, "A mathematical theory of communication," *Bell Syst. Tech. J.*, vol. 27, no. 3, pp. 379–423, 1948.

[56] S. R. Cloude and E. Pottier, "A review of target decomposition theorems in radar polarimetry," *IEEE Trans. Geosci. Remote Sens.*, vol. 34, no. 2, pp. 498–518, Mar. 1996.

[57] C. Szigarski et al., "Analysis of the radar vegetation index and potential improvements," *Remote Sens.*, vol. 10, no. 11, 2018, Art. no. 1776.

[58] Y. Kim and J. J. van Zyl, "A time-series approach to estimate soil moisture using polarimetric radar data," *IEEE Trans. Geosci. Remote Sens.*, vol. 47, no. 8, pp. 2519–2527, Aug. 2009.

[59] D. Ratha, S. De, T. Celik, and A. Bhattacharya, "Change detection in polarimetric SAR images using a geodesic distance between scattering mechanisms," *IEEE Geosci. Remote Sens. Lett.*, vol. 14, no. 7, pp. 1066–1070, Jul. 2017.

[60] O. Antropov, Y. Rauste, and T. Hame, "Volume scattering modeling in PolSAR decompositions: Study of ALOS PALSAR data over boreal forest," *IEEE Trans. Geosci. Remote Sens.*, vol. 49, no. 10, pp. 3838–3848, Oct. 2011.

[61] D. Ratha, D. Mandal, V. Kumar, H. McNairn, A. Bhattacharya, and A. C. Frery, "A generalized volume scattering model-based vegetation index from polarimetric SAR data," *IEEE Geosci. Remote Sens. Lett.*, vol. 16, no. 11, pp. 1791–1795, Nov. 2019.

[62] E. M. Kennaugh, "Effects of the type of polarization on echo characteristics," Antenna Lab, Ohio State University, Columbus, OH, USA, Tech. Rep. 389-9, 1951.

[63] D. Fernandes and A. C. Frery, "Statistical properties of geodesic distances between samples and elementary scatterers in PolSAR imagery," in *Proc. IEEE Recent Adv. Geosci. Remote Sens., Technol. Standards Appl.*, 2019, pp. 11–14.

[64] D. W. Marquardt, "An algorithm for least-squares estimation of nonlinear parameters," *J. Soc. Ind. Appl. Math.*, vol. 11, no. 2, pp. 431–441, 1963.

[65] M. T. Hallikainen, F. T. Ulaby, M. C. Dobson, M. A. El-Rayes, and L.-K. Wu, "Microwave dielectric behavior of wet soil—Part 1: Empirical models and experimental observations," *IEEE Trans. Geosci. Remote Sens.*, vol. GE-23, no. 1, pp. 25–34, Jan. 1985.

[66] A. Züfle, K. Wessels, and D. Pfoser, "Mining high resolution Earth observation data cubes," in *Proc. 17th Int. Symp. Spatial Temporal Databases*, 2021, pp. 152–156.

[67] N. Bhogapurapu et al., "Soil moisture retrieval over croplands using dual-pol L-band GRD SAR data," *Remote Sens. Environ.*, vol. 271, 2022, Art. no. 112900.

[68] G. G. Ponnurangam, T. Jagdhuber, I. Hajnsek, and Y. Rao, "Soil moisture estimation using hybrid polarimetric SAR data of RISAT-1," *IEEE Trans. Geosci. Remote Sens.*, vol. 54, no. 4, pp. 2033–2049, Apr. 2016.

[69] D. Mandal, A. Bhattacharya, and Y. S. Rao, "Evolution of semi-empirical approach: Modeling and inversion," in *Radar Remote Sensing for Crop Biophysical Parameter Estimation*. Berlin, Germany: Springer, 2021, pp. 73–106.

[70] L. Zhang, X. Lv, Q. Chen, G. Sun, and J. Yao, "Estimation of surface soil moisture during corn growth stage from SAR and optical data using a combined scattering model," *Remote Sens.*, vol. 12, no. 11, 2020, Art. no. 1844.

[71] T. Riedel, C. Pathe, C. Thiel, M. Herold, and C. Schmullius, "Systematic investigation on the effect of dew and interception on multifrequency and multipolarimetric radar backscatter signals," in *Retrieval of Bio-and Geo-Physical Parameters From SAR Data for Land Applications*. Noordwijk, The Netherlands: ESA Publications, 2002, pp. 99–104.

[72] X. Bai, D. Zheng, X. Liu, L. Fan, J. Zeng, and X. Li, "Simulation of Sentinel-1A observations and constraint of water cloud model at the regional scale using a discrete scattering model," *Remote Sens. Environ.*, vol. 283, 2022, Art. no. 113308.

[73] A. Muhuri et al., "Performance assessment of optical satellite-based operational snow cover monitoring algorithms in forested landscapes," *IEEE J. Sel. Topics Appl. Earth Observ. Remote Sens.*, vol. 14, pp. 7159–7178, Jun. 2021.

[74] H.S. Srivastava, P. Patel, Y. Sharma, and R. R. Navalgund, "Large-area soil moisture estimation using multi-incidence-angle RADARSAT-1 SAR data," *IEEE Trans. Geosci. Remote Sens.*, vol. 47, no. 8, no. 8, pp. 2528–2535, Aug. 2009.

[75] S. S. Ghosh, S. Dey, N. Bhogapurapu, S. Homayouni, A. Bhattacharya, and H. McNairn, "Gaussian process regression model for crop biophysical parameter retrieval from multi-polarized C-band SAR data," *Remote Sens.*, vol. 14, no. 4, 2022, Art. no. 934.

[76] M. Xing et al., "Retrieving surface soil moisture over wheat and soybean fields during growing season using modified water cloud model from Radarsat-2 SAR data," *Remote Sens.*, vol. 11, no. 16, 2019, Art. no. 1956.

[77] J. Shi, J. Wang, A. Y. Hsu, P. E. O'Neill, and E. T. Engman, "Estimation of bare surface soil moisture and surface roughness parameter using L-band SAR image data," *IEEE Trans. Geosci. Remote Sens.*, vol. 35, no. 5, pp. 1254–1266, Sep. 1997.

[78] X. Zhang, B. Chen, H. Fan, J. Huang, and H. Zhao, "The potential use of multi-band SAR data for soil moisture retrieval over bare agricultural areas: Hebei, China," *Remote Sens.*, vol. 8, no. 1, 2015, Art. no. 7.

[79] G. Macelloni et al., "The SIR-C/X-SAR experiment on Montespertoli: Sensitivity to hydrological parameters," *Int. J. Remote Sens.*, vol. 20, no. 13, pp. 2597–2612, 1999.

[80] S. Paloscia, G. Macelloni, P. Pampaloni, and E. Santi, "The contribution of multitemporal SAR data in assessing hydrological parameters," *IEEE Geosci. Remote Sens. Lett.*, vol. 1, no. 3, pp. 201–205, Jul. 2004.

**Arnab Muhuri** holds a Bachelors in Electrical Engineering (2009) and later obtained his Master of Technology (2012) & PhD (2018) in Satellite Earth Observation from the Indian Institute of Technology (IIT) Bombay, India. In 2018, for his research contributions, he was conferred upon the Excellence in PhD Research Award by the Honorable Prime Minister of India, Shri. Narendra Modi, at the 56th Institute Convocation of IIT Bombay, India.

In 2019, he was awarded the Alexander von Humboldt (AvH) Fellowship by the AvH Foundation, Government of the Federal Republic of Germany, to continue his research at the Professur für Hydrogeographie und Klimatologie, Geographisches Institut, Universität Heidelberg. In 2020, he was awarded the European Research Stay Grant by the AvH Foundation for working as a Visiting Scientist at the Centre d'Etudes Spatiales de la Biosphére (CESBIO)-Centre National d'Etudes Spatiales (CNES), Toulouse, France. In 2021, he joined the Centre d'Applications et de Recherches en Télédétection (CARTEL) at L'Université de Sherbrooke, Québec, Canada where his research was funded by the Discovery grant and CREATE program of the Natural Sciences and Engineering Research Council of Canada (NSERC). In 2022, he joined the Earth Observation and Modelling (EOM), Geographisches Institut, Christian-Albrechts-Universität zu Kiel, Germany, where he is working towards his Habilitation and teaches courses on satellite Earth observation. His present research interests lies in the development of Earth observation algorithms integrating fundamentals of imaging physics with information retrieval techniques like machine learning for applications like grassland and coastal monitoring with SAR, LiDAR, and optical sensors.

Dr. Muhuri has collaboratively worked with the Space Application Center (SAC), Indian Space Research Organisation (ISRO), and Defence Research & Development Organisation (DRDO), Ministry of Defence, Government of India. He was a Visiting Fellow at the University of Tokyo, Japan under the DST-JSPS grant. Dr. Muhuri has worked with Earth observation (RADARSAT-2 and RADARSAT Constellation Mission (RCM)) and extra-terrestrial (Chandrayaan-1 Mini-SAR) satellite missions for interdisciplinary applications like exploration of the Lunar polar regions, high-mountain cryosphere monitoring, natural disaster impact assessment, agricultural parameter retrieval, and development of polarimetric SAR decomposition techniques. He is on the review board of IEEE TGRS & JSTARS, International Journal of Climatology, Remote Sensing of Environment etc. and serves as a Research Ambassador for Heidelberg Alumni International, Universität Heidelberg.

**Kalifa Goïta** received the Engineering degree in surveying engineering from the École Nationale d'Ingénieurs, Bamako, Mali, in 1987, and the M.Sc. and Ph.D. degrees in remote sensing from the Université de Sherbrooke, Sherbrooke, QC, Canada, in 1991 and 1995, respectively.

From 1995 to 1997, he was a Postdoctoral Fellow with the Climate Research Branch of Environment Canada, Toronto, ON, Canada. From 1997 to 2002, he was a Professor of remote sensing and GIS with the Faculty of forestry, Université de Moncton, Moncton, NB, Canada. Since June 2002, he has been a Professor of geomatics with the Université de Sherbrooke, where he was the Head of the Department of Applied Geomatics from 2009 to 2014, and has been the Director of the Remote Sensing Research Centre (Centre d'applications et de recherches en télédétection, CARTEL) since 2015. He has supervised/co-supervised numerous master, Ph.D. students, and postdoctoral researchers, and is the author/coauthor of several research papers in the broad field of environmental remote sensing and water resources. His research interests include environmental geomatics, microwave remote sensing of soil moisture and snow, as well as satellite gravimetry and altimetry applied to water resources.

**Ramata Magagi** received the B.Sc. degree in physics from the Université de Niamey, Niamey, Niger, in 1989, and the M.Sc. and Ph.D. degrees in physics and chemistry of environment from the Institut National Polytechnique de Toulouse, Toulouse, France, in 1992 and 1995, respectively.

She led the Canadian Experiment for Soil Moisture in 2010 (CanEx-SM10). She is currently a Professor with the Department of Applied Geomatics, Université de Sherbrooke, Sherbrooke, QC, Canada. Her research interests included active and passive microwave remote sensing of soil, snow, vegetation, and precipitation.

**Hongquan Wang** received the B.Sc. degree in geographic information systems from the Northeast Forestry University, Harbin, China, in 2007, the M.Sc. degree in silviculture (forest remote sensing) from the Chinese Academy of Forestry, Beijing, China, in 2010, and the Ph.D. degree in synthetic aperture radar (SAR) remote sensing from the National Institute of Applied Sciences, IETR CNRS-6164, Rennes, France, in 2014.

He was involved in several scientific projects in the framework of CNRS Zone Atelier Armorique in France. From 2014 to 2018, he was a Postdoctoral Fellow with the Center for Research and Application of Remote Sensing (CARTEL), University of Sherbrooke, Sherbrooke, QC, Canada, where he participated in the Soil Moisture Active Passive Validation Experiments in 2012 and 2016. From 2018 to 2021, he was an Assistant Professor with the Department of Environment and Resource Science, Zhejiang University, Hangzhou, China. As a Principal Investigator, he led several research programs to develop remote sensing models, algorithms, and applications to characterize hydrosphere, cryosphere, biosphere, ecosystem, and climate changes. Since 2021, he has been a Researcher with the University of Sherbrooke and then with Agriculture and Agri-Food Canada (AAFC), Edmonton, AB, Canada. His research interests include the development of multisource remote sensing (radar, radiometer, multispectral, hyperspectral, and lidar) methodologies (e.g., polarimetric decompositions, radiative transfer models), and applications to characterize the dynamics of the Earth system.